Graphical Abstract

Flux organizations and control modes in antagonistically combined negative feedback loops

Peter Ruoff

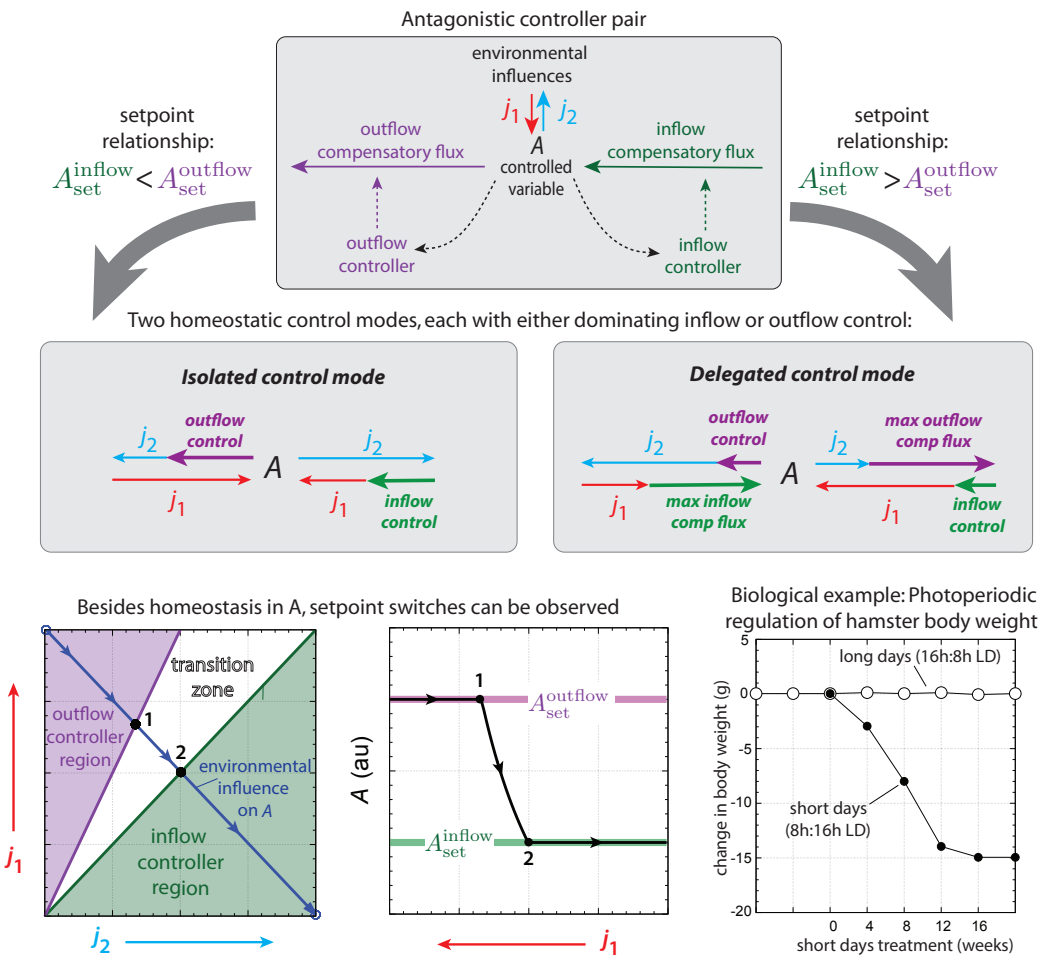

Highlights

Flux organizations and control modes in antagonistically combined negative feedback loops

Peter Ruoff

- A set of 16 inflow/outflow controllers (negative feedbacks) combined by a common controlled variable have been studied.
- Dependent on the relationship between the inflow/outflow controllers' setpoints two distinct regulatory modes termed 'delegated control' and 'isolated control' have been identified.
- Regions of control and their extensions are visualized by a 'perturbation phase diagram'.
- Metastable control may temporarily occur when one of the controller variables are environmentally increased or decreased.
- Robust perfect or near-perfect adaptation may occur even in the absence of integral feedback.
- The combined controllers can show homeostatic as well as rheostatic behaviors. A striking biological example of rheostasis is found in the photoperiodic regulation of the Siberian hamster's body weight.
- The origin of the glycemic setpoint in blood glucose homeostasis is still debated. A glucagon- and insulin-based two-setpoint model suggests that in diabetic individuals the upper insulin-dependent setpoint increases with decreasing insulin generation rates. This setpoint is defended irrespective of its value, but the accuracy of regulation depends how tightly the insulin degrading enzyme (IDE, insulysin) binds to insulin. In addition, both glucagon- and insulin-based setpoints depend (rheostatically) on the level of somatostatin.

Flux organizations and control modes in antagonistically combined negative feedback loops

Peter Ruoff

University of Stavanger, Department of Chemistry, Bioscience, and Environmental Engineering, Kjell Arholms gate 41, Stavanger, 4021, Rogaland, Norway

Abstract

The purpose of this paper is to show the different compensatory responses and control models towards environmental perturbations when two antagonistic integral controllers are combined at the level of the controlled variable. Dependent on the controllers' relative setpoints two types of compensatory flux regulations occur, which have been termed delegated and isolated control. In delegated control one of the feedbacks submits its entire compensatory flux to the system, while the other feedback is the actual controller by neutralizing the excess flux of its antagonistic partner. In isolated control the compensatory flux of one of the controllers is negligible while the other feedback regulates the controlled variable alone. One of the findings is that these interacting feedbacks can exhibit environmentally driven setpoint changes known as rheostasis. A striking example is the photoperiodic control of Siberian hamsters' body weights, which can be rationalized by the interacting feedbacks between circadian morning (M) and evening (E) oscillators. A third control type is metastable control. Here, additions or removals of the controller variable can cause a switch to the antagonistic partner's control regime, but resets to its original control mode once additions or removals stop. Integral windup can induce temporary metastable setpoint changes or even lead to robust perfect adaptation without integral feedback! How the setpoint in blood glucose homeostasis arises is still debated. A dual-controller approach with two setpoints can describe many properties of blood glucose homeostasis and the roles of insulin, glucagon, and somatostatin.

Keywords: negative feedback, integral control, homeostasis, rheostasis, windup, metastability, blood glucose regulation, body weight control

1. Introduction

The term 'homeostasis' was introduced by Walter Cannon (Cannon, 1929, 1939; Langley, 1973) to address the ability of organisms to defend themselves against internal and external disturbances. This is done by keeping their physiological steady states within narrow limits (Clancy and McVicar, 2002; Billman, 2020). Wiener's cybernetics and the findings that negative feedback mechanisms play a major role in homeostatic regulation (Curtis et al., 1958; Hughes, 1964) were the start to describe homeostasis and adaptation mechanisms by combined methods from control engineering and reaction kinetics. The success to describe homeostatic mechanisms by feedback regulation led some researchers to equate homeostasis with single negative feedback regulations and a defined constant setpoint. However, the facets of homeostasis involve more than regulation by a single negative feedback loop. Thus, alternative terminologies were introduced. Selye (1974) coined the term 'heterostasis' to point to alternative regulations when a control system faces unusually high demands. The term 'enantiostasis' was introduced by Mangum and Towle (1977) to describe a preserved relationship between an environmental influence and a regulated variable (Hochachka and Somero, 1984). Moore-Ede (1986), focussing on the anticipatory adaptation of circadian rhythms, introduced the term 'predictive homeostasis' to include regulations by these biochemical oscillators. The term 'rheostasis', introduced by Mrosovsky (1990), points to the fact that homeostatic setpoints may change dependent on environmental conditions and may include the regulation by circadian or other biochemical oscillators on a hierarchical basis (Stevenson, 2024).
'Allostasis' (Schulkin, 2003, 2004), a term suggested by Sterling and Eyer (1988) and closely connected to the concept of rheostasis, focuses on coordinated changes in the brain by neural signaling pathways, which may include setpoint changes with respect to external conditions, such as environmental stress. Although these aspects of homeostatic regulation, such as changes of setpoints, suggested hierarchical organization (Stevenson, 2024), or the presence of nonlinear dynamics (Lloyd et al., 2001), are clearly important, they still fall within Cannon's original definition. As argued by Carpenter (2004) and as discussed at the end of the paper with respect to rheostasis, Cannon's homeostasis definition can still serve as a unifying concept.

Physiological controllers come often in antagonistic pairs and regulate

inflow and outflow fluxes to and from a homeostatic controlled compound. Blood glucose regulation by insulin and glucagon is one of many examples. Saunders' 'rein control' model (Saunders et al., 1998, 2000) is an example of how antagonistic compensatory fluxes induced by insulin and glucagon contribute to an overall blood glucose homeostasis.

In the present work I combine integral inflow and outflow feedbacks, such that each feedback has a defined setpoint and contributes to the regulation of the controlled variable. Fig 1 shows how controller combinations are arranged. Unlike hierarchical control arrangements (Thorsen et al., 2018; Nygård and Ruoff, 2023) there is no 'cross-talk' between the inflow and outflow controllers. Compound A is the controlled variable which is influenced by the environmental perturbations k_1 and k_2. During homeostasis, but dependent on k_1 and k_2, A can be kept at the setpoint of one of the controllers or in-between these setpoints.

The signaling between A and the individual controllers is described by

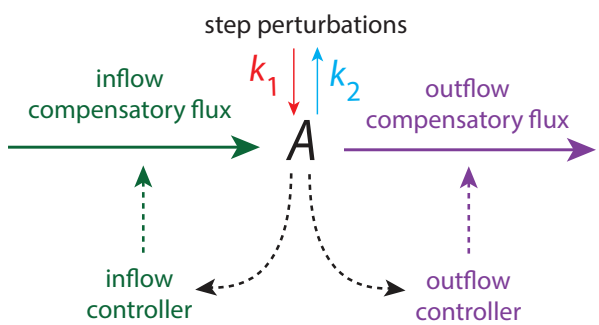

Figure 1: The arrangement of the investigated combinations between inflow and outflow controllers to keep homeostasis in A. Dependent on the step perturbations k_1 and k_2 (indicated respectively as red and blue arrows), inflow and/or outflow controllers (outlined in green and violet) will be activated to maintain A homeostasis. Dashed lines indicate signaling from A to the controllers and the activation of the compensatory fluxes.

saturation kinetics, i.e. by activation or inhibition of a compensatory flux. Thus, control of A may break down when perturbations become too large and compensatory fluxes reach their maximum limits (Ang et al., 2010).

2. Materials and methods

2.1. Computational methods

Computations were performed with the Fortran subroutine LSODE (Radhakrishnan and Hindmarsh, 1993) with plots generated by gnuplot (www.gnuplot.info). Reaction schemes and plot annotations were prepared with Adobe Illustrator (www.adobe.com). Rate constants and other parameters are in arbitrary units (au) and represented by k_1, k_2, k_3,... independent of their kinetic meaning, i.e. whether they are turnover numbers, Michaelis constants, or activation/inhibition constants.

2.2. The studied individual controllers (negative feedbacks)

Because many physiological controllers come in antagonistic pairs, I have looked at the combinations between inflow and outflow controllers (Ni et al., 2009; Drengstig et al., 2012a), which act directly on the controlled variable as indicated in Fig 1. Fig 2 shows a set of eight single-loop negative feedback loops (Drengstig et al., 2012a), which have been employed in this study. In these feedbacks integral control is achieved by zero-order kinetic removal of the E_i ('control of the controller principle' (Ni et al., 2009); see section 2.5 for further details). The eight feedbacks divide into two equal sets which have been termed inflow and outflow controllers (Fig 2). The controlled variable and its concentration is described as A, while the controller variables are the E_i's, where i identifies one of the eight controller motifs Mi with $i \in \{1, 2, .., 7, 8\}$.

2.3. Implementation of inhibition and activation

Inhibitions of a reaction rate r by X (here X is A, or E_k with $k \in \{1, 2, .., 7, 8\}$) is achieved by multiplying r with the inhibition factor f_{inhib}

$$r_{inhibited} = r \cdot f_{inhib} = r \cdot \frac{k_{inhib}}{k_{inhib} + X} \tag{1}$$

where k_{inhib} is a inhibition constant. Kinetically this is equivalent to what is known as a special case of 'mixed inhibition' (Segel, 1975), where two inhibition constants have the same value and are written as one.

Activations are described by two scenarios. In the first one activation is described in terms of a 'mixed activation' (Cornish-Bowden, 2004) by activator Y with activation constant k_{act}, i.e.

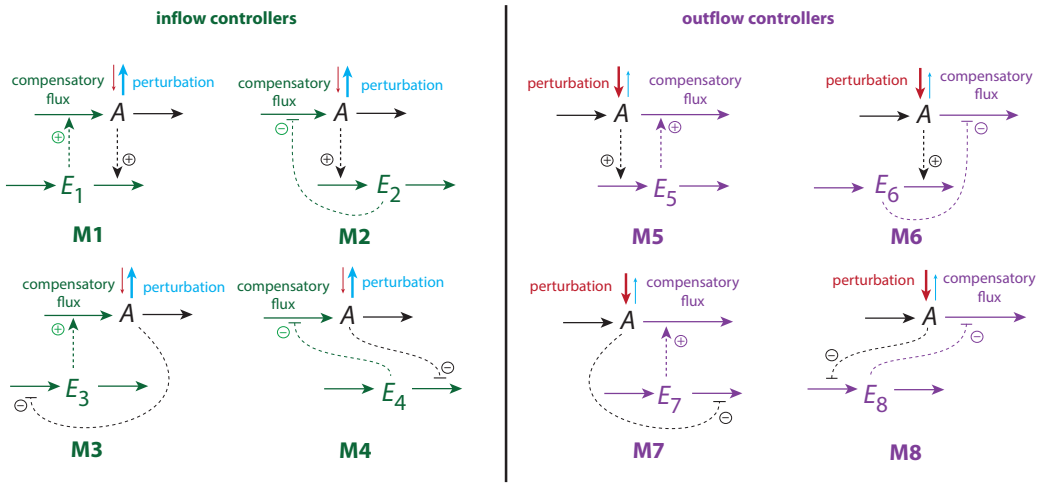

Figure 2: The eight negative feedback loops used in this study. The four inflow controllers M1-M4 are combined with the four outflow controllers M5-M8 which leads to sixteen possible combinations (see below). A is the controlled variable while the E_i's ($i = 1, 2, .., 8$) are the controller (manipulated) variables. Dashed lines indicate the signaling between A and the E_i's in terms of activations (plus signs) or inhibitions (minus signs). It may be mentioned that a similar negative feedback classification was used by Franck in his 1980 paper on physicochemical oscillators (see Fig 4 in Franck (1980)).

$$r_{activated} = r \cdot f_{act} = r \cdot \frac{Y}{k_{act} + Y} \tag{2}$$

In the other scenario we have first-order kinetics with respect to the activator Y, i.e.

$$r_{activated} = r' \cdot Y \tag{3}$$

This approach avoids saturation by Y in Eq 2 and saturation-related breakdowns (Ang and McMillen, 2013).

To compare the effects between these two activation types I have included computations when *activated compensatory fluxes* use either Eq 2 or Eq 3. It may be noted that first-order activation with respect to activator Y (Eq 3) represents a special case of Eq 2, i.e. when k_{act} becomes much larger than Y and r' can be written as $r'{=}r/k_{act}$. As k_{act} is a dissociation constant (the Michaelis constant K_M) between the binding of the activator Y and an enzyme catalyzing reaction r Eq 3 reflects a 'low-affinity' activation and

regulation. On the other hand, Eq 2 can be considered as a 'high-affinity' regulation when k_{act} is low. The distinction between high-affinity and low-affinity kinetics is well documented for transport proteins, and may also be used to distinguish compensatory fluxes in homeostatic regulations (for an example, see Huang et al. (2011)).

It should be further mentioned that these formulations represent simplifications and that biochemical activations and inhibitions are generally more complex, as they often involve positive or/and negative cooperativities Segel (1975), along possible hysteretic or allosteric behaviors (Frieden, 1970; Farnsworth, 2025). Such complexities are neglected here.

2.4. Keeping oscillatory behavior of feedbacks at a minimum

Although oscillations are often observed in biological systems, I decided to focus here on nonoscillatory regulation and keep oscillatory behavior at a minimum. It is well known that negative feedbacks can oscillate (Goodwin, 1963; Franck, 1980; Kholodenko, 2000; Goldbeter et al., 2001; Pigolotti et al., 2007; Jolma et al., 2010), especially when aggressiveness (or loop-gain) of the feedback is increased (Blanchini et al., 2018), or when the removal of the controlled variable becomes zero-order with respect to A. In the latter case the average of the controlled variable can show robust perfect adaptation when integral control is present (Thorsen et al., 2014). Since first-order removals with respect to the controlled variable A can effectively quench oscillatory behavior of a negative feedback (Thorsen et al., 2014) (but not always ovoid it) all A removals are formulated in this study as first-order reactions with respect to A.

2.5. Implementation of integral control

Since the start of cybernetics during the middle of the 20th century there is now a repeated interest to understand the molecular and topological aspects behind perfect (and near perfect) adaptations and its relevance for homeostasis in biochemical/physiological systems or synthetic biology (Barkai and Leibler, 1997; Saunders et al., 1998, 2000; Yi et al., 2000; Levchenko and Iglesias, 2002; Ni et al., 2009; Drengstig et al., 2008; Ang et al., 2010; Iglesias and Ingalls, 2010; Araujo and Liotta, 2018; Krishnan and Floros, 2019; Aoki et al., 2019; Khammash, 2021; Hirono et al., 2023;

Ponsiglione et al., 2023; Bhattacharya et al., 2024; Andrews et al., 2024; Hirono et al., 2025).

To ensure that the combined controllers show robust homeostasis with respect to a defined setpoint of the controlled variable I implemented integral control into the negative feedbacks. Integral control is a concept from control engineering (Warwick, 1996; Wilkie et al., 2002; Yi et al., 2000; Iglesias and Ingalls, 2010), which allows to regulate a controlled variable via a negative feedback precisely to a defined setpoint independent of step perturbations that are applied to the controlled variable. Integral feedback results in so-called 'robust perfect adaptation', unless the feedback encounters certain physical constraints (Ang et al., 2010).

Fig 3a illustrates the mechanism of integral control. The function $f(A)$ of a controlled variable A (outlined in blue), is compared with the red outlined fixed reference A_{ref}. The error, i.e. the difference $A_{ref}-f(A)$ is calculated and integrated in time. The integrated error, often multiplied with a gain factor, results in E (outlined in green), which is then fed into the process to counteract stepwise perturbations applied to A. The general proof of this method can be found in textbooks (see for example Warwick (1996) or Wilkie et al. (2002)).

Fig 3b shows how zero-order degradation of E_7 incorporates integral control in motif M7 and defines the setpoint of A. The color coding in Fig 3b corresponds to that in panel a indicating the contributions of the individual rate parameters to reach integral control. For motif M7 the reference function $f(A)$ is the strength of A's inhibition on E_7's degradation. With respect to the other motifs $f(A)$ may be simply A or be described by an activation of the form $K_a/(K_a+A)$. When the error goes to zero A settles at its setpoint, which can be deduced from the relationship $f(A)=A_{ref}$. The condition $\dot{E}_7=[A_{ref}-f(A)]$ in Fig 3b shows that E is proportional to the integrated error and A inhibits the degradation of E_7 with constant strength. To show when integral control is working properly and when controller breakdown occurs, a phase diagram is employed, which divides the perturbation space into regions of control, their transitions, and regions of breakdown (see section 'Perturbation phase diagram' below).

The usage of zero-order (or near zero-order) kinetics in the removal of

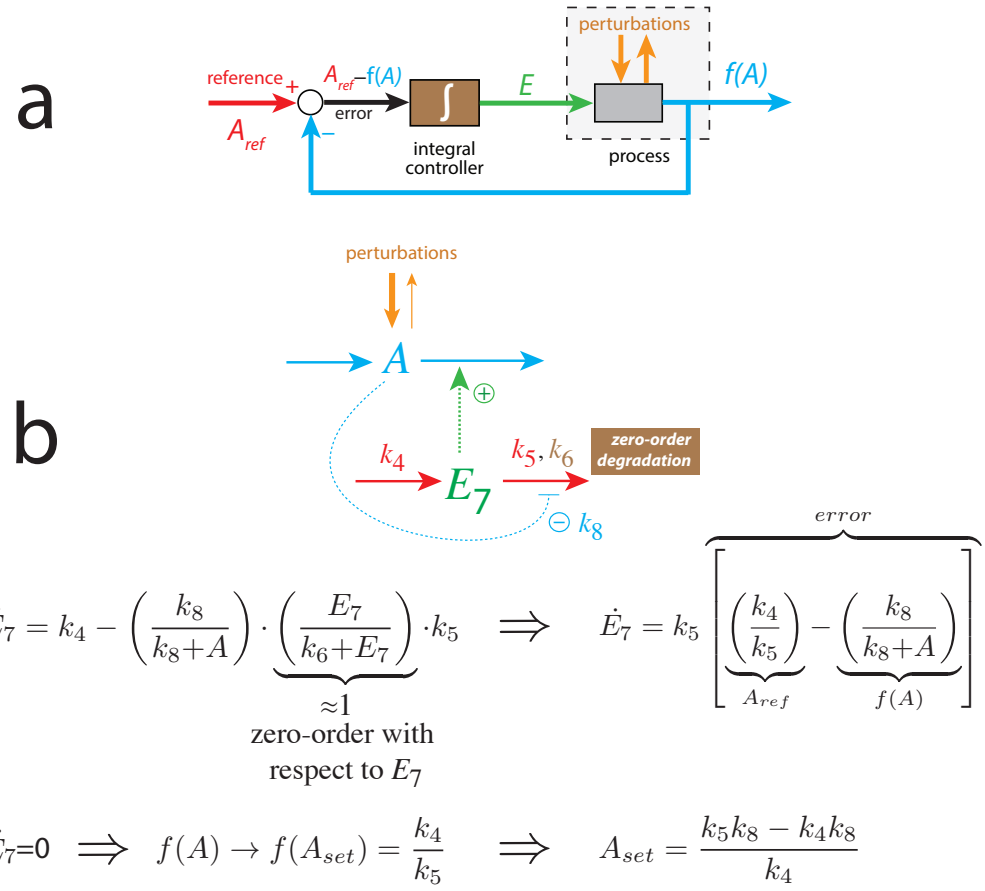

$$\dot{E}_7 = k_4 - \left(\frac{k_8}{k_8+A}\right) \cdot \underbrace{\left(\frac{E_7}{k_6+E_7}\right)}_{\substack{\approx 1 \\ \text{zero-order with} \\ \text{respect to } E_7}} \cdot k_5 \quad \Longrightarrow \quad \dot{E}_7 = k_5 \overbrace{\left[\underbrace{\left(\frac{k_4}{k_5}\right)}_{A_{ref}} - \underbrace{\left(\frac{k_8}{k_8+A}\right)}_{f(A)}\right]}^{error}$$

$$\dot{E}_7 = 0 \quad \Longrightarrow \quad f(A) \rightarrow f(A_{set}) = \frac{k_4}{k_5} \quad \Longrightarrow \quad A_{set} = \frac{k_5 k_8 - k_4 k_8}{k_4}$$

Figure 3: Mechanism of integral control. Panel a: General scheme to obtain integral control. The output $f(A)$ is subtracted from the reference A_{ref} and integrated. The integrated error E is then fed into the negative feedback with the result to oppose perturbations acting on the controlled variable A. The setpoint of A is obtained from the relationship $f(A)=A_{ref}$ by solving for A. Panel b: Motif M7 (Fig 2) is used as an illustration with color coding corresponding to panel a. The reaction scheme shows the motif with zero-order degradation of E_7 by using a low k_6. In all calculations a value of 1.0×10^{-6} is used. It reflects a strong binding between the E_i's (here E_7) and a putative E_i-removing/processing enzyme. When $f(A)=A_{ref}$ steady state of A is reached with A at its setpoint A_{set}.

E_i can be interpreted in form of E_i-processing enzymes which work under saturation or near saturation conditions (Ni et al., 2009; Drengstig et al., 2008). In this respect, the Michaelis constants of these enzymes are closely related to the accuracy/inaccuracy of the controlling feedbacks (Drengstig

et al., 2012a).

Other mechanisms to achieve integral control employs first-order autocatalysis in association with a first-order removal of the controller variable E_i (Shoval et al., 2010; Drengstig et al., 2012b; Briat et al., 2016; M. Zand et al., 2024). This type of integral control implementation is generally fast (Nishiyama et al., 2023) and can counteract perturbations which increase rapidly in time (Fjeld et al., 2017).

In addition, topological methods have been put forward to achieve or predict robust perfect adaptation (Levchenko and Iglesias, 2002; Drengstig et al., 2008; Shinar and Feinberg, 2010; Araujo and Liotta, 2018, 2023; Hirono et al., 2023; Bhattacharya et al., 2024; Andrews et al., 2024; Hirono et al., 2025).

2.6. Integral windup

Windup is observed as a continuous growth or decrease in the controller variable E_i (see supplementary material in Drengstig et al. (2012a), p.22ff). Here, it will be shown that windup, besides leading to controller breakdown can even result in homeostatic behaviors.

2.7. The combined feedbacks

Fig 4 shows the sixteen inflow/outflow controller combinations between the eight feedback motifs of Fig 2. The individual inflow/outflow controllers act directly on A by their respective compensatory fluxes.

2.8. Perturbation phase diagram

To characterize the homeostatic behaviors of the combined controllers I make use of a *perturbation phase diagram*. The diagram, schematically outlined in Fig 5, consists of regions of control and breakdown as a function of the perturbations k_1 and k_2. Depending on the individual controllers' setpoints and their signaling kinetics a *transition zone* between the regions of control may be observed. The regions of control and the transition zone are separated by border lines, which are described by linear equations of the form

$$k_1 = a \cdot k_2 + b \tag{4}$$

where a and b depend on the rate constants and setpoints of the combined Mi's. The derivations of the borderlines are described in detail in the main

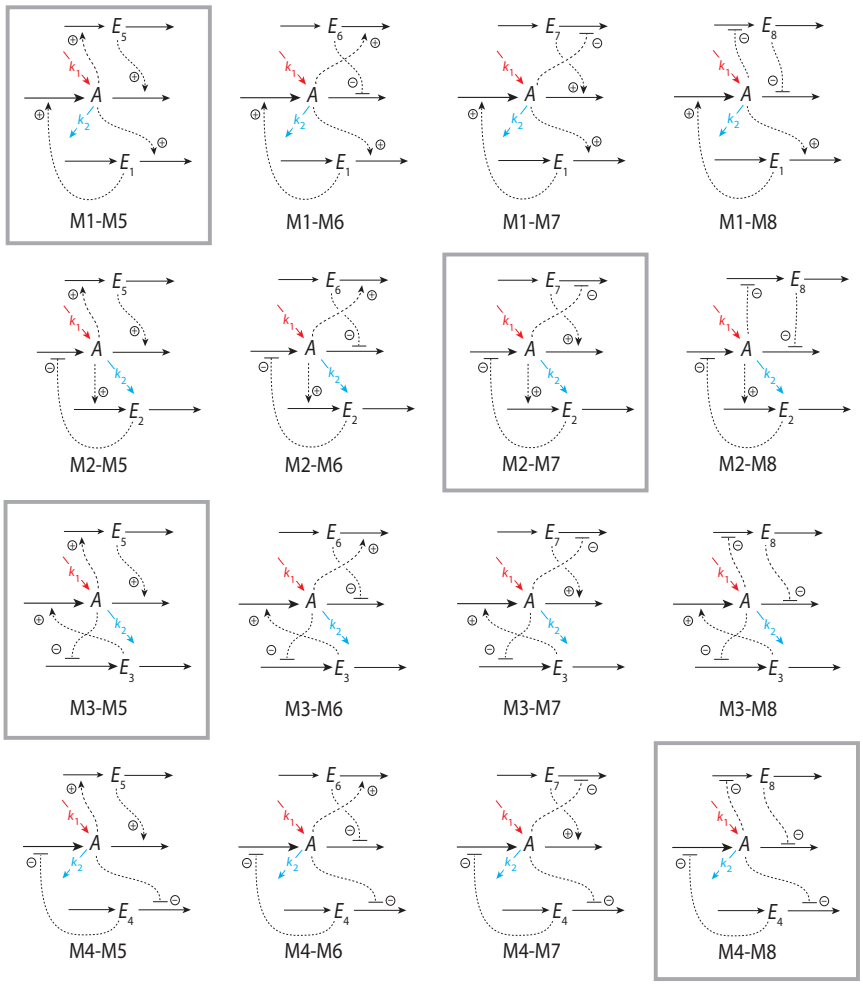

Figure 4: An overview of the sixteen combinations between inflow and outflow controllers. A synopsis of all controller combinations with the conditions for delegated and isolated control is found in the supplementary material Sup1.pdf. The framed schemes are described in detail in the main text (combination M1-M5), and in the supplementary material Sup2.pdf (combinations M2-M7, M3-M5, and M4-M8).

text for combination M1-M5 and in the supplementary material Sup2.pdf for the combinations M2-M7, M3-M5, and M4-M8.

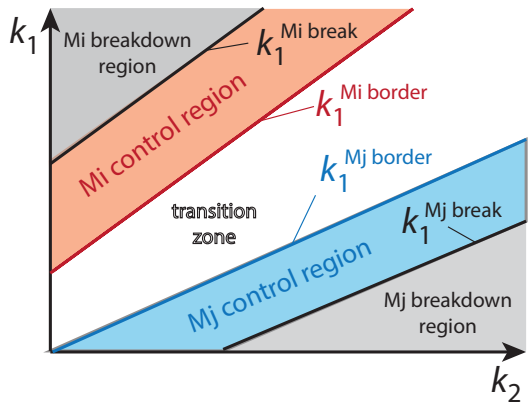

Figure 5: Outline of a perturbation phase diagram between combined controllers Mi and Mj. Ordinate and abscissa indicate the values of k_1 and k_2 perturbations acting on A (see Fig 1). The regions of A-control by Mi and Mj are outlined in red and blue, respectively. A transition zone (outlined in white) which separates the two control regions may be present. The two controllers' breakdown regions are indicated in grey. $k_1^{Mi/j\,break}$ and $k_1^{Mi/j\,border}$ describe the borders (Eq 4) between the controlled regions and the breakdown regions, and the borders between the controlled regions and the transition zone, respectively.

3. Results

3.1. Overview

First, a brief outline of delegated and isolated control is given with detailed descriptions of the combined M1-M5 controller's features. The supplementary material `Sup1.pdf` provides a brief overview of all controller combinations with setpoints, windup behaviors, and borderlines. In addition, supplementary material `Sup2.pdf` gives more detailed descriptions of the M2-M7, M3-M5, and M4-M8 controller combinations. Then 'metastable control' is described with examples in the main text and in supplementary material `Sup3.pdf`. This is followed by a chapter how robust homeostasis may even occur in open-loop designs without integral feedback.

At the end of the paper two biological examples are discussed in relationship with combined antagonistic feedbacks having different setpoints. One example concerns the photoperiodic regulation of the Siberian hamster's body weight in terms of combined feedbacks between evening (E) and morning (M) circadian oscillators. The other example shows how blood glucose homeostasis can be understood on basis of an insulin- and glucagon-based

two-setpoint mechanism and how the setpoints are affected by somatostatin.

The four supplementary files `Sup4.mp4-Sup7.mp4` show animations to illustrate how the rate constants of inflow and outflow compensatory fluxes affect controllers' borderlines and their control regions. For documentation, a selected set of the Fortran results are provided in Python code.

3.1.1. Flux organization in delegated control

Delegated control occurs when the setpoint of the inflow controller is larger than the setpoint of the outflow controller. Dependent on the values of k_1 and k_2 A can be controlled either by the inflow or by the outflow controller, meaning that the steady state concentration of A is either at $A_{ss}{=}A_{set}^{inflow}$ or at $A_{ss}{=}A_{set}^{outflow}$. In case an outflow controller controls A at $A_{set}^{outflow}$ (the four motifs M5 to M8) the inflow controller will submit its fully developed compensatory flux to the system. We can distinguish two cases: (i) For inflow compensatory fluxes based on activation/deactivation (motifs M1 or M3) the compensatory fluxes take the form (Eq 2; see also Tables S1-S4 and S9-S12 in supplementary material Sup1.pdf):

$$j_{comp}^{inflow} = j_{comp,\,max}^{inflow}\left(\frac{E_i}{K_a{+}E_i}\right) \Rightarrow j_{comp}^{inflow} = j_{comp,\,max}^{inflow}, \quad i \in \{1,3\} \qquad (5)$$

with positive windup in both E_1 or E_3, i.e. $\dot{E}_1{>}0$ or $\dot{E}_3{>}0$. (ii) For inflow compensatory fluxes based on repression/derepression (motifs M2 or M4) we have (Eq 1; Tables S5-S8 and S13-S16 (Sup1.pdf)):

$$j_{comp}^{inflow} = j_{comp,\,max}^{inflow}\left(\frac{K_I}{K_I{+}E_i}\right) \Rightarrow j_{comp}^{inflow} = j_{comp,\,max}^{inflow}, \quad i \in \{2,4\} \qquad (6)$$

with negative windup in both E_2 or E_4, i.e. $\dot{E}_2{<}0$ or $\dot{E}_4{<}0$.

On the other hand, when the inflow controller determines A ($A_{ss}{=}A_{set}^{inflow}$, motifs M1-M4), it is the outflow controller which contributes with its fully developed compensatory flux. Also here we distinguish between compensatory fluxes based on activation (M5 or M7) and compensatory fluxes based on repression/derepression (M6 or M8). For the outflow compensatory fluxes

based on activation/deactivation they take the form (see also Tables S1, S5, S9, and S13; and S3, S7, S11, and S15 in Sup1.pdf)

$$j_{comp}^{outflow} = j_{comp\,max}^{outflow}\left(\frac{E_i}{K_I+E_i}\right) \Rightarrow j_{comp}^{outflow} = j_{comp\,max}^{outflow}, \quad i \in \{5,7\} \tag{7}$$

with positive windup in both E_5 or E_7, i.e. $\dot{E}_5>0$ or $\dot{E}_7>0$. For the compensatory fluxes based on repression/derepression (motifs M6 and M8) we get (see also Tables S2, S6, S10, and S14; and S4, S8, S12, and S16 (Sup1.pdf))

$$j_{comp}^{outflow} = j_{comp\,max}^{outflow}\left(\frac{K_I}{K_I+E_i}\right) \Rightarrow j_{comp}^{outflow} = j_{comp\,max}^{outflow}, \quad i \in \{6,8\} \tag{8}$$

with negative windup in both E_6 or E_8, i.e. $\dot{E}_6<0$ or $\dot{E}_8<0$.
Fig 6 illustrates the regulation of the compensatory fluxes under delegated control. In panel a the outflow controller (outlined in violet) regulates the concentration of A to $A_{set}^{outflow}$ while the combined inflow controller will contribute with its maximum compensatory flux (outlined in green). Perfect adaptation at $A_{set}^{outflow}$ is kept as long as increasing inflow perturbations can be met with increased outflow compensatory fluxes, while increasing outflow perturbations can be balanced by decreased outflow compensatory fluxes. Panel b shows the situation when an inflow controller regulates the concentration of A at A_{set}^{inflow}. In this case the connected outflow controller will contribute with its maximum compensatory flux and the inflow controller will adjust its compensatory flux according to the inflow/outflow perturbations. Controller breakdown occurs whenever adjusted compensatory fluxes have either reached their maximum capacities or have become zero.

3.1.2. Flux organization in isolated control

Isolated control occurs when the outflow controller's setpoint is larger than the setpoint of the inflow controller. For example, when the outflow controller moves A to its setpoint (A_{ss}=$A_{set}^{outflow}$) the inflow compensatory flux becomes negligible, practically zero. The reason for this is that for inflow compensatory fluxes based on activation/deactivation (M1 or M3) the corresponding E_i's undergo negative windup ($\dot{E}_1<0$ or $\dot{E}_3<0$) such that (see also Tables S17 to S20, and S25 to S28 in Sup1.pdf)

$$j_{comp}^{inflow} = j_{comp\,max}^{inflow}\left(\frac{E_i}{K_a+E_i}\right) \Rightarrow j_{comp}^{inflow} \to 0, \quad i \in \{1,3\} \tag{9}$$

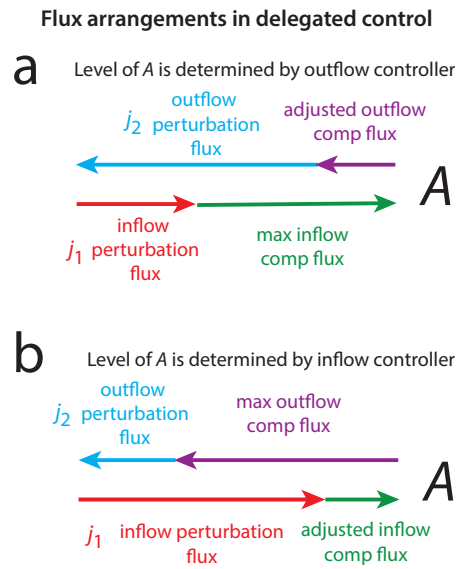

Figure 6: Compensatory flux arrangements in delegated control. Delegated control occurs when the setpoint of the inflow controller is larger than the setpoint of the outflow controller. Panel a: When the outflow controller determines the steady state of A at $A_{set}^{outflow}$ the inflow controller contributes with its maximum compensatory flux (outlined in green). To keep homeostasis in A the outflow controller adjusts its compensatory flux (outlined in violet) in dependence how inflow/outflow perturbations to or from A change (outlined in red and blue). Panel b: When the inflow controller determines the level of A the outflow controller's compensatory flux is at its maximum (outlined in violet) while the green inflow controller's compensatory flux is adjusted according to the level of the inflow/outflow perturbations (outlined in red and blue).

For the inflow compensatory fluxes based on repression/derepression (M2 or M4) the corresponding E_i's show positive windup ($\dot{E}_2$>0 or $\dot{E}_4$>0; see also Tables S21 to S24, and S29 to S32 in Sup1.pdf), which leads to

$$j_{comp}^{inflow} = j_{comp\,max}^{inflow} \left(\frac{K_I}{K_I + E_i} \right) \Rightarrow j_{comp}^{inflow} \to 0, \quad i \in \{2, 4\} \tag{10}$$

When the inflow controller determines the steady state concentration of A at A_{ss}=A_{set}^{inflow} the outflow compensatory flux is negligible, i.e. the inflow controller determines the concentration of A alone. Here, outflow compensatory fluxes based on activation/deactivation (M5 or M7) show negative windup ($\dot{E}_5$<0 or $\dot{E}_7$<0; Tables S17, S21, S25, and S29; and Tables S19, S23,

S27, and S31 in Sup1.pdf) which leads lead to

$$j_{comp}^{outflow} = j_{comp\,max}^{outflow}\left(\frac{E_i}{K_I+E_i}\right) \Rightarrow j_{comp}^{outflow} \to 0, \quad i \in \{5,7\} \tag{11}$$

while outflow compensatory fluxes based on repression/derepression (M6 or M8) show positive windup ($\dot{E}_6$>0 or $\dot{E}_8$>0; Tables S18, S22, S26, and S30; and Tables S20, S24, S28, and S32 in Sup1.pdf) leading likewise to

$$j_{comp}^{outflow} = j_{comp\,max}^{outflow}\left(\frac{K_I}{K_I+E_i}\right) \Rightarrow j_{comp}^{outflow} \to 0, \quad i \in \{6,8\} \tag{12}$$

Fig 7 summarizes the compensatory flux behaviors in isolated control. In panel a the outflow controller determines A at $A_{set}^{outflow}$ with a negligible compensatory flux of the combined inflow controller; the outflow controller solely controls A when inflow perturbations dominate. In panel b an outflow perturbation is dominating and the inflow controller determines A at A_{set}^{inflow}. The combined outflow controller does not contribute in the regulation of A and has a negligible compensatory flux.

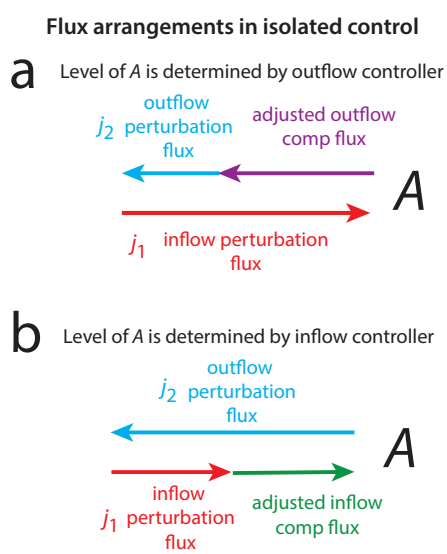

Figure 7: Compensatory flux arrangement in isolated control when A_{set}^{inflow}<$A_{set}^{outflow}$. Panel a: When inflow perturbations to A dominate, the level of A is determined by the outflow controller (its compensatory flux is outlined in violet) and the inflow controller stays silent; its compensatory flux is negligible. The situation is reversed in panel b when an outflow perturbation from A dominates and the inflow controller (its compensatory flux is outlined in green) determines the level of A without any significant compensatory flux from the outflow controller.

3.2. Combined M1 and M5 controllers

In the following the dynamic behaviors and perturbation phase diagrams of combined M1 and M5 controllers are described in dependence to the set-points of the two controllers. Fig 8 shows the reaction scheme.

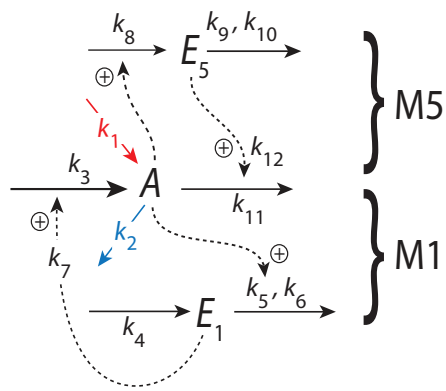

Figure 8: The combined M1-M5 controller. Outlined in red and blue indicate the stepwise inflow (k_1) and outflow (k_2) perturbations applied to A. M1 and M5 work by directly activating their respective compensatory fluxes j_3 and j_{11} with activation constants k_7 and k_{12} (Eq 13). A on its side activates the removal of E_1 and the synthesis of E_5 by first-order reactions with respect to A.

The rate equations are:

$$\dot{A} = \underbrace{k_1}_{\text{perturbation}} - \underbrace{k_2 \cdot A}_{\text{perturbation}} + \underbrace{k_3 \left(\frac{E_1}{k_7 + E_1} \right)}_{\text{M1 compensatory flux } j_3} - \underbrace{k_{11} \cdot A \left(\frac{E_5}{k_{12} + E_5} \right)}_{\text{M5 compensatory flux } j_{11}} \tag{13}$$

$$\dot{E}_1 = k_4 - k_5 \cdot \underbrace{\left(\frac{E_1}{k_6 + E_1} \right)}_{\approx 1,\, \text{low } k_6} \cdot A \tag{14}$$

$$\dot{E}_5 = k_8 \cdot A - k_9 \cdot \underbrace{\left(\frac{E_5}{k_{10} + E_5} \right)}_{\approx 1,\, \text{low } k_{10}} \tag{15}$$

Activation of M1's and M5's compensatory fluxes j_3 and j_{11} involve activation constants k_7 and k_{12}, respectively. Activations by A are described by first-order processes with respect to A. Integral control by the M1 and M5

controllers are introduced by zero-order kinetics with respect to E_1 (Eq 14) and E_5 (Eq 15), which give $E_1/(k_6+E_1)$ and $E_5/(k_{10}+E_5)$ ratios close to 1. Practically this is done by setting k_6 and k_{10} to 1×10^{-6}. From Eqs 14 and 15 the setpoints of the M1 and M5 controllers are then found to be, respectively,

$$A_{set}^{M1} = \frac{k_4}{k_5} \tag{16}$$

$$A_{set}^{M5} = \frac{k_9}{k_8} \tag{17}$$

3.2.1. Delegated control ($A_{set}^{M1}>A_{set}^{M5}$)

To illustrate delegated control A_{set}^{M1} is set (rather arbitrarily) to 2.0 and A_{set}^{M5} to 1.0. When M1 controls A M5 contributes with a fully developed compensatory flux ($j_{11}=k_{11}\cdot A_{set}^{M1}$, Eq 13) by windup of E_5. E_5 windup occurs because A is kept lower than A_{set}^{M5}, which leads to $\dot{E}_5>0$ (Eq 15; see also Table S1 in Sup1.pdf). On the other hand, when M5 controls A, E_1 goes into windup since A is now kept lower than A_{set}^{M1} thereby resulting in $\dot{E}_1>0$. Thus, M1 contributes with its entire compensatory flux $j_3=k_3$ (Eq 13; Table S1, Sup1.pdf). The controller which actively regulates A does so by adjusting/reducing its compensatory flux in order to neutralize the exceeding compensatory inflow or outflow fluxes by the other controller (illustrated in Fig 6).

Fig 9a shows the perturbation phase diagram with four different k_1 and k_2 combinations during four phases which alternate between M5 and M1 control (panels b-d). Typically, the windup of E_1 or E_5 during respective M5 control (phases 1 and 3) or M1 control (phases 2 and 4) causes increased settling times of A in response to the changed setpoint (indicated by the logarithmic time scale in Figs 9b-d).

Borderlines in M1-M5 delegated control. The four borderlines between regions of control, breakdown, and the transition zone are indicated in Fig 9a. The greyed M1 breakdown region 'M1 br' is characterized by a low/insufficient M1 compensatory flux $j_3 \cong 0$ and a high A-dependent M5 compensatory flux, which is approximately described by $j_{11}=k_{11}A$. Thus, during M1 breakdown,

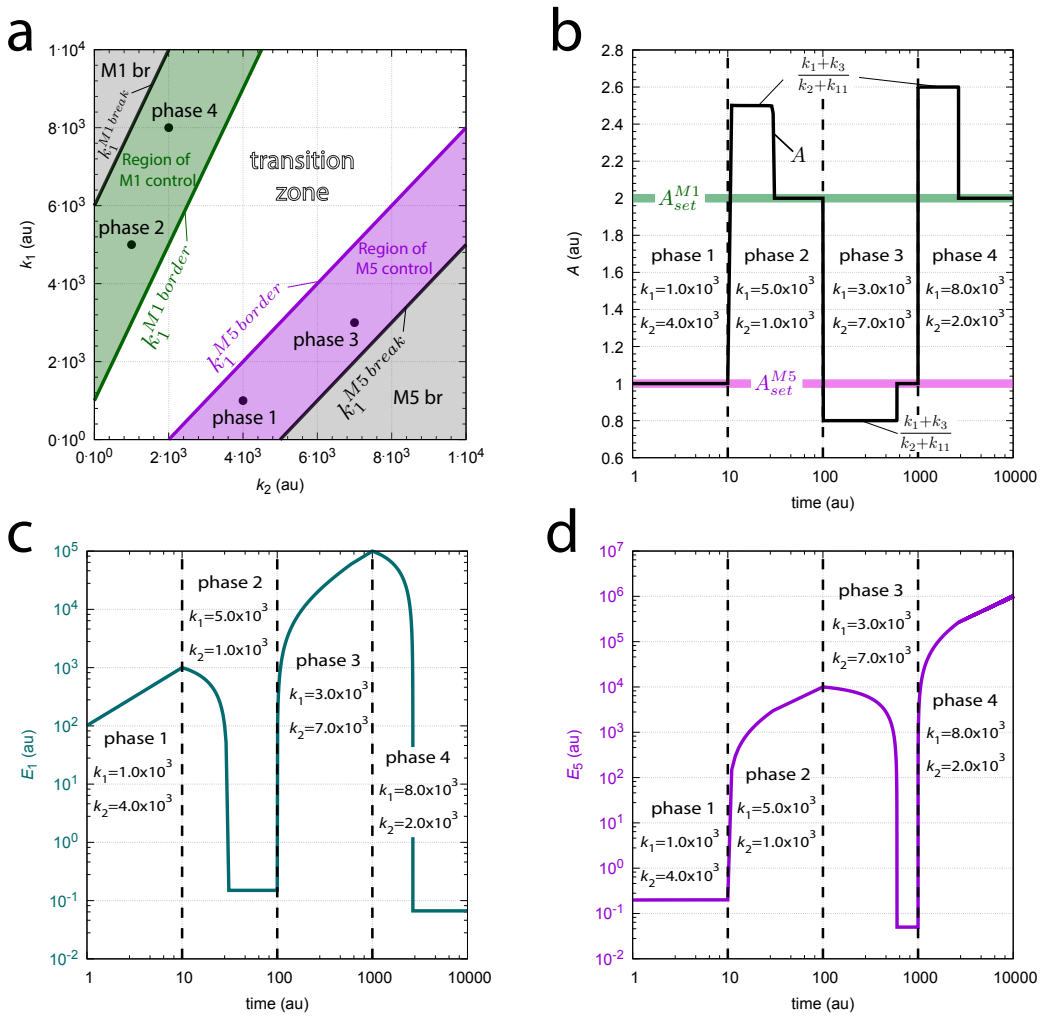

Figure 9: Example of delegated control in the combined M1-M5 controller when A_{set}^{M1}=2.0 and A_{set}^{M5}=1.0. Panel a shows the perturbation phase diagram indicating the (k_2, k_1) values during the four phases when alternating between M5 and M1 control. Panel b: A as a function of time during the four phases. The temporary A-plateaus prior A reaches its setpoint occur because j_3 and j_{11} become temporarily saturated. The values of these plateaus can be calculated by Eq 21 below. Panel c: E_1 as a function of time. Panel d: E_5 as a function of time. Note the logarithmic times scales in panels b-d. Rate constants: k_3=5.0×10^3, k_4=200.0, k_5=100.0, k_6=1.0×10^{-6}, k_7=0.1, k_8=100.0, k_9=100.0, k_{10}=1.0×10^{-6}, k_{11}=3.0×10^3, k_{12}=0.1. Initial concentrations: A_0=1.0, $E_{1,0}$=1.57, and $E_{5,0}$=0.1. See Python code for details.

A becomes dependent upon k_1 and k_2, which is approximately described by

$$A_{ss} = \frac{k_1}{k_2 + k_{11}} \tag{18}$$

The borderline '$k_1^{M1\,break}$', which separates the greyed M1 breakdown region from the green 'Region of M1 control', shows k_1 as a function of k_2, which is characterized by M5's high compensatory flux at A_{ss}=A_{set}^{M1} and M1's incapability to further neutralize $j_{comp,\,max}^{M5}$=$k_{11}A_{set}^{M1}$: j_3 is approximately zero. Inserting these conditions into Eq 13 with steady state in A leads to the expression how k_1 depends on k_2 along the border, i.e.

$$k_1^{M1\,break} = (k_2 + k_{11})\cdot A_{set}^{M1} \tag{19}$$

'$k_1^{M1\,border}$', which separates the region of M1 control (outlined in green) and the transition zone (white region), is characterized that both M1 and M5 compensatory fluxes are fully developed, i.e. j_{comp}^{M1}=j_3=k_3 and j_{comp}^{M5}=j_{11}=$k_{11}A_{ss}$. Inserting these conditions into the rate equation of A and setting the steady state at A_{ss}=A_{set}^{M1} leads to the k_1-k_2 relationship

$$k_1^{M1\,border} = (k_2 + k_{11})\cdot A_{set}^{M1} - k_3 \tag{20}$$

The 'Region of M1 control' is characterized by M5's fully developed compensatory flux j_{11}=$k_{11}A_{set}^{M1}$. However, dependent on the k_1 and k_2 values M1's compensatory flux is adjusted in such a way that it neutralizes j_{11} and thereby keeps A_{ss} at A_{set}^{M1}. In the transition zone both M1 and M5 have maximum developed compensatory fluxes, but A's steady state depends on both k_1 and k_2, i.e.

$$A_{ss} = \frac{k_1 + k_3}{k_2 + k_{11}} \tag{21}$$

'$k_1^{M5\,border}$' describes the k_1-k_2 relationship when M1 and M5 compensatory fluxes are both at their maxima, but M5 has just gained control over A with A_{ss}=A_{set}^{M5}:

$$k_1^{M5\,border} = (k_2 + k_{11})\cdot A_{set}^{M5} - k_3 \tag{22}$$

In the 'Region of M5 control' M1's compensatory flux is at its maximum, but now M5 adjusts its compensatory flux such that A_{ss} can be kept at A_{set}^{M5}. The border '$k_1^{M5\,break}$' separates the region of M5 control from its breakdown region 'M5 br', i.e. when M5's compensatory flux j_{11} becomes negligible. Assuming that $j_{11} \approx 0$ this border is described by

$$k_1^{M5\,break} = k_2\cdot A_{set}^{M5} - k_3 \tag{23}$$

Taking that within the M5 breakdown region M5's compensatory flux is approximately zero the steady state of A becomes dependent upon k_1 and k_2 described by

$$A_{ss} = \frac{k_1 + k_3}{k_2} \tag{24}$$

M1-M5 delegated control: Moving across the perturbation phase diagram. To test the above expressions of the borderlines and to view the behaviors of the compensatory fluxes one can look at the system when perturbations move along a trajectory across the perturbation phase diagram. Fig 10 shows the changes of A, E_1, E_5, and the compensatory fluxes j_3 and j_{11} when k_1, k_2 values change along the blue straight line indicated in panel a. In the M1 breakdown region 'M1 br' (panel a) M1 cannot compensate the high A-dependent M5 compensatory flux $j_{11}{=}k_{11}A$. In this region A decreases as k_1 decreases and k_2 increases (panel b) according to Eq 18. At point '1' the trajectory crosses the '$k_1^{M1\,break}$' border. Within the region of M1 control E_1 and the compensatory flux j_3 increase. In other words, M1 now adjusts its compensatory flux to keep A at A_{set}^{M1} as k_1 and k_2 change. M5's compensatory flux is now high and constant, described by $j_{11}{=}k_{11}A_{set}^{M1}$ (panel d, right ordinate). When crossing '$k_1^{M1\,border}$' at point '2' and entering the transition zone M1's compensatory flux j_3 is at its maximum value k_3. M5's compensatory flux decreases and A decreases in dependence of k_1 and k_2 according to Eq 21. Entering the M5 controlled region at point '3' keeps A at A_{set}^{M5} as M5 adjust its compensatory flux while j_3 is at its maximum. Finally, when entering the M5 breakdown region 'M5 br', A control by M5 collapses and A decreases according to Eq 24.

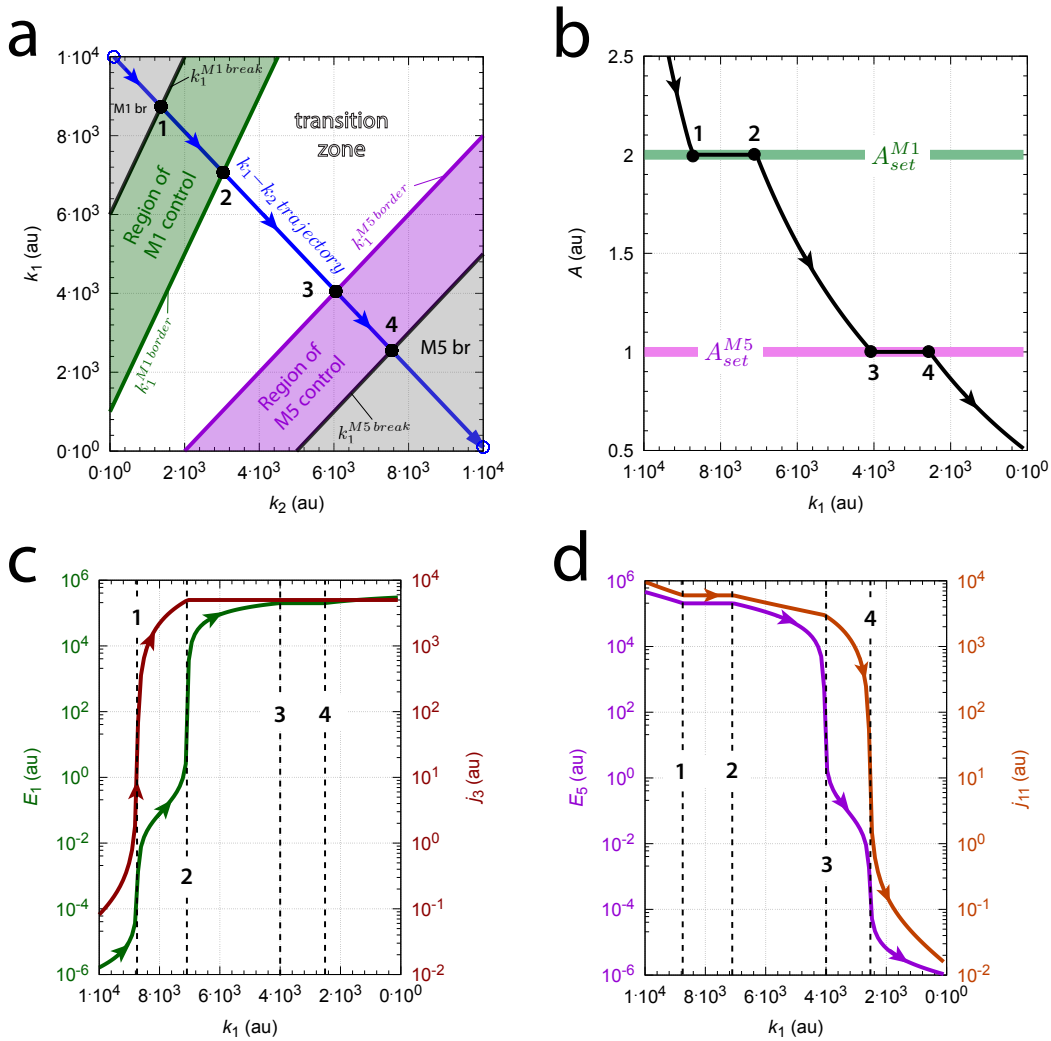

Figure 10: Values of A, E_1, and E_5 calculated along a straight line across the perturbation phase diagram (outlined in blue, panel a). Start values: k_1^{start}=1.0×10^4, k_2^{start}=1.0×10^2. End values: k_1^{end}=1.0×10^2, k_2^{end}=1.0×10^4. The calculation was performed by dividing the line into 100 data points and determining the values of A, E_1, and E_5 after 2000 time units for each point (to ensure steady state in A). Panel b: A steady state values as a function of (decreasing) k_1. Panel c: E_1 (left ordinate) and compensatory flux j_3 (right ordinate) as a function of k_1. Panel d: E_5 (left ordinate) and compensatory flux j_{11} (right ordinate) as a function of k_1. Solid black points and vertical dashed lines show the calculated k_1, k_2 intersection points between the blue trajectory and the border lines Eqs 19, 20, 22, and 23. Rate constants as in Fig 9. Start concentrations (for all 100 data points): A=3.226, E_1=1.63×10^{-6}, and E_5=22.26.

3.2.2. Isolated control (A_{set}^{M1}<A_{set}^{M5})

When A_{set}^{M1}<A_{set}^{M5} the combined M1-M5 controller shows isolated control. In this case, dependent on the perturbations, either M1 alone, or M5 alone controls A while the other controller remains silent. Fig 11 shows a calculation for A_{set}^{M1}=1.0 and A_{set}^{M5}=2.0 with five different k_1, k_2 perturbations/phases. The regions of M1 and M5 control, the transition zone, and the regions of the controllers' breakdown is illustrated in the phase diagram shown in panel a.

In the transition zone both controllers have 'shut down' with practically zero compensatory fluxes. The A concentration inside the transition zone is therefore described by the ratio k_1/k_2. Panel b shows the concentration of A during the five phases. Panels c and d show respectively E_1 and E_5 as a function of time. Windup of E_1 and E_5 is only observed in respectively phase 5 and phase 1 when M1 or M5 controllers have broken down.

The borderlines between the different regions inside the phase diagram can be rationalized as follows. The $k_1^{M1\,break}$ border between M1 control (outline in green, Fig 11a) and M1 breakdown (lower greyed region) has a low/negligible M5 compensatory flux (j_{11}≈0), but a maximum (saturated) M1 compensatory flux (j_3=k_3) with windup in E_1. Inserting these conditions into Eq 13, and allowing steady state conditions in A, leads to the $k_1^{M1\,break}$ border expressed as a function of k_2:

$$k_1^{M1\,break} = k_2 \cdot A_{set}^{M1} - k_3 \tag{25}$$

Concerning the borders between the M1 and M5 control regions and the transition zone, termed $k_1^{M1\,border}$ and $k_1^{M5\,border}$, both M1 and M5 controllers are inactive with negligible compensatory fluxes j_3 and j_{11}. This leads respectively to Eqs 26 and 27:

$$k_1^{M1\,border} = k_2 \cdot A_{set}^{M1} \tag{26}$$

$$k_1^{M5\,border} = k_2 \cdot A_{set}^{M5} \tag{27}$$

The border $k_1^{M5\,break}$ between the region of M5 control (outlined in violet in Fig 11a) and M5 breakdown (upper greyed region 'M5 br') is characterized by a completely saturated M5 compensatory flux j_{11}=$k_{11}A_{set}^{M5}$ with E_5 windup and a negligible M1 compensatory flux j_3≈0, which leads to the expression:

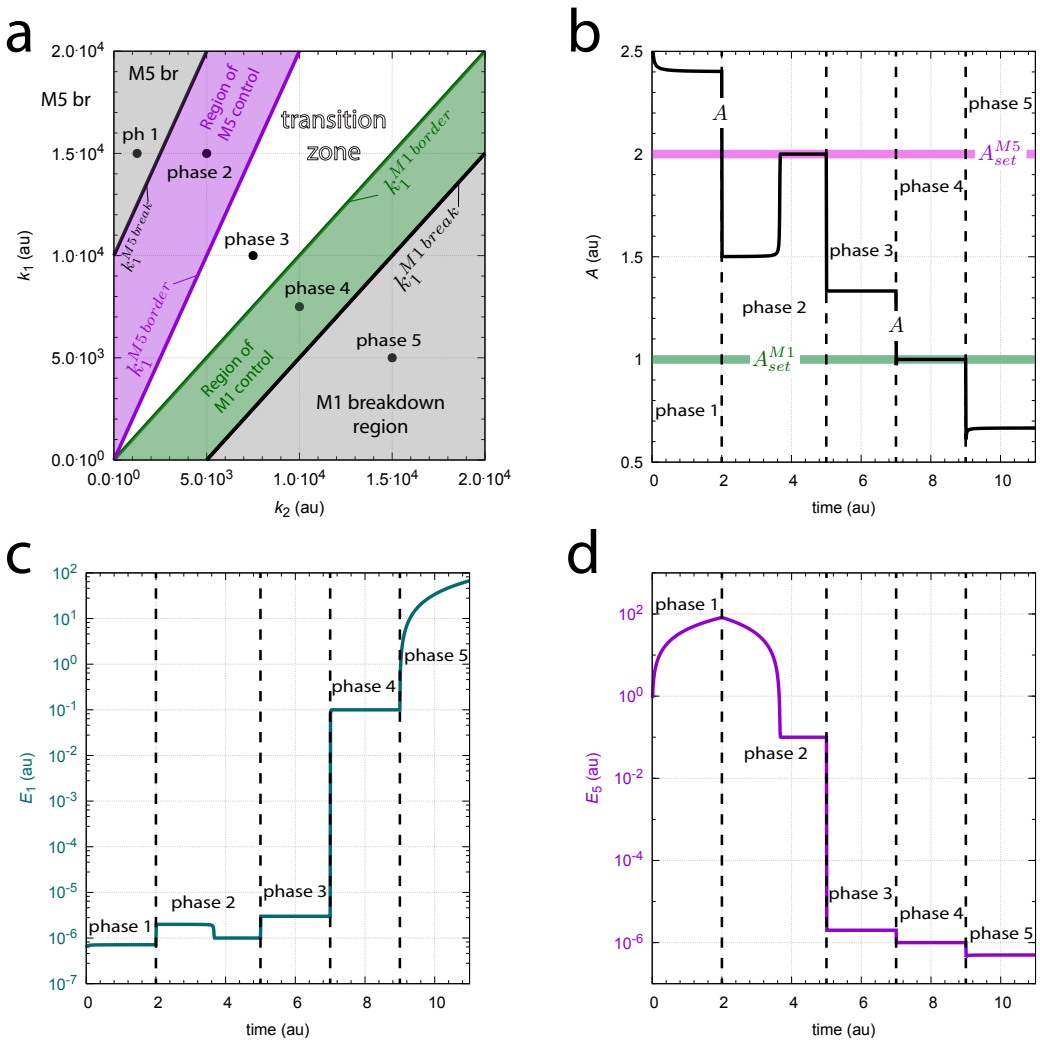

Figure 11: Example calculation of isolated control when A_{set}^{M1}=1.0 and A_{set}^{M5}=2.0. Panel a: Perturbation phase diagram with regions of M1 and M5 control (colored respectively in green and violet) and their greyed breakdown regions. In the calculation five k_1, k_2 perturbations were applied. Phase 1 (ph 1): k_1=1.5×10^4, k_2=1.25×10^3; phase 2: k_1=1.5×10^4, k_2=5.0×10^3; phase 3: k_1=1.0×10^4, k_2=7.5×10^3; phase 4: k_1=7.5×10^3, k_2=1.0×10^4; phase 5: k_1=5.0×10^3, k_2=1.5×10^4. Panel b: Concentration of A as a function of time. Panel c: Concentration of E_1 as a function of time. Panel d: Concentration of E_5 as a function of time. Note that the duration of phase 2 has been increased to allow E_5 to reach a concentration where M5 can exert control on A. Rate constants: k_3=5.0×10^3, k_4=100.0, k_5=100.0, k_6=1.0×10^{-6}, k_7=0.1, k_8=100.0, k_9=200.0, k_{10}=1.0×10^{-6}, k_{11}=5.0×10^3, k_{12}=0.1. Initial concentrations: A_0=2.4046, $E_{1,0}$=7.12×10^{-7}, and $E_{5,0}$=0.0. See Python code for details.

$$k_1^{M5\,break} = (k_2 + k_{11})\cdot A_{set}^{M5} \tag{28}$$

M1-M5 isolated control: Moving across the perturbation phase diagram. To test the validity of the borderline expressions Eqs 25-28 Fig 12 shows a calculation across the perturbation phase diagram along a straight line, which is indicated in blue (see panel a). The calculation starts out at high k_1 (2.0×10^4) and low k_2 (1.0×10^2) values and ends at low k_1 (1.0×10^2) and high k_2 (2.0×10^4) values. The line was divided into 100 data points and for each point the steady states of A were calculated. Panel b shows the numerically calculated A values as a function of (decreasing) k_1. In addition, the solid dots 1-4 in panels a and b show the calculated intersection points between the blue line and the borderline expressions Eqs 25-28.

Fig 12c shows E_1 (left ordinate) and its compensatory flux j_3 (right ordinate) as a function of decreasing k_1. The k_1 values at the intersection points 1-4 are indicated as vertical dashed lines. Note the relative large changes of E_1 and j_3 at points 3 and 4 indicating active M1 control while the M5 compensatory j_{11} (panel d) is negligible. Likewise, during M5 control between points 1 and 2 j_{11} varies significantly to obtain A homeostasis (panel d), while M1's compensatory flux does not contribute to the homeostasis (panel c). Fig 12d shows the corresponding E_5 and j_{11} values as a function of decreasing k_1. During M5 control (crossing points 1 and 2) there is a large change in E_5 and compensatory flux j_{11}, while during M1 control (crossing points 3 and 4) E_5 and j_{11} are low and constant. Comparing panels c and d shows the 'isolated control type' by M1 or M5, i.e. the absence of any significant compensatory flux by one of the controller when the other one is in charge to keep A at its setpoint.

3.2.3. $A_{set}^{M5} \rightarrow A_{set}^{M1}$: Switching from isolated to delegated control

I wondered how the system would respond when A_{set}^{M1} and A_{set}^{M5} become identical. Would the system behave somewhat between delegated and isolated control? To investigate this question the controllers were compared when A_{set}^{M1} and A_{set}^{M5} are close (but the system still shows isolated control), and when A_{set}^{M1} and A_{set}^{M5} have become equal. Fig 13 (panels a1-a4) show the system's behavior when A_{set}^{M1}=1.0 and A_{set}^{M5}=1.1. Panel a1 shows the perturbation phase diagram with the k_1 and k_2 values changing along the blue straight line. The other panels (a2-a4) show A, E_1, j_3, E_5, and j_{11} as a

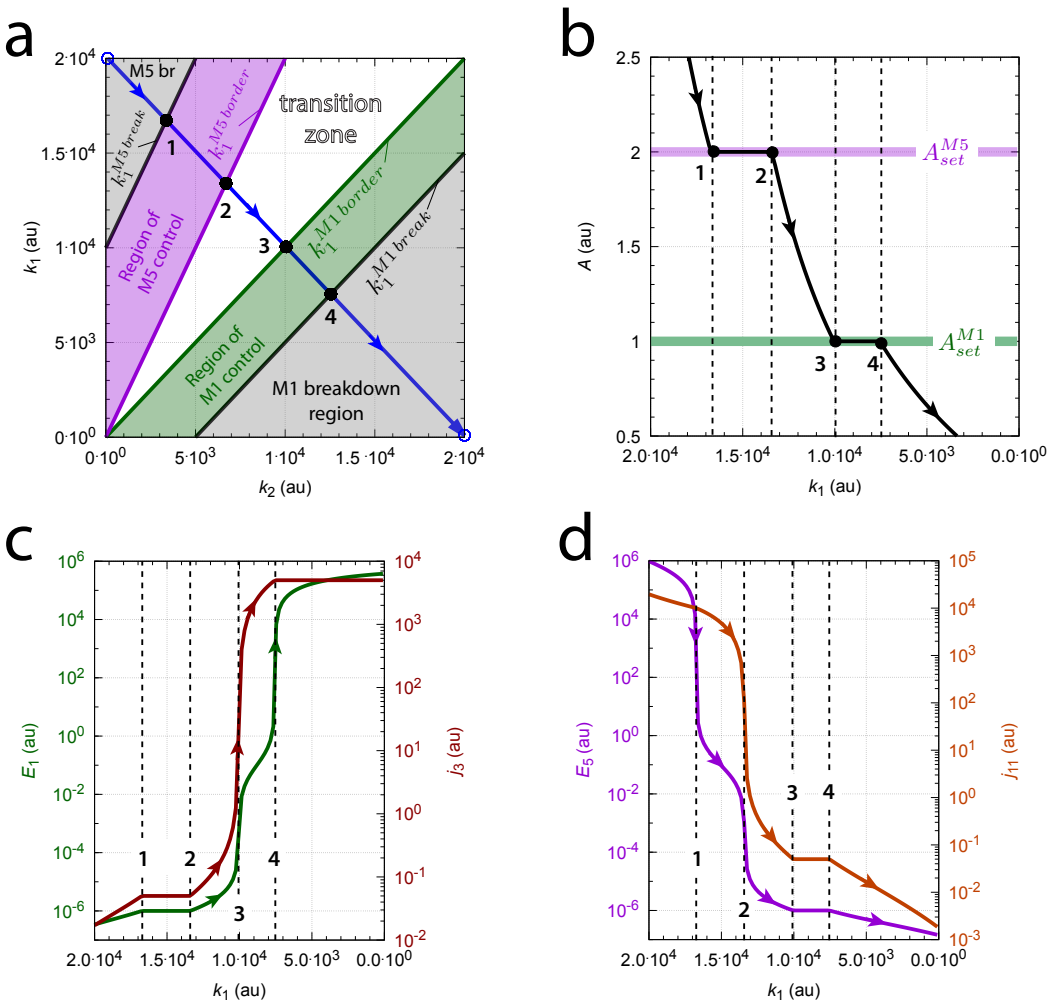

Figure 12: Moving across the perturbation phase diagram at isolated M1-M5 control. Panel a: Perturbation phase diagram. Start values: k_1^{start}=2.0×10^4, k_2^{start}=1.0×10^2. End values: k_1^{end}=1.0×10^2, k_2^{end}=2.0×10^4. The blue line indicates the path of calculation. The path was divided into 100 sections and for each section the steady states of A, E_1, and E_5 were calculated after 5000 time units. Solid black dots and numbers show the calculated intersection points with the borderlines Eqs 25-28. Panel b: A as a function of (decreasing) k_1. Panel c: E_1 (left ordinate) and compensatory flux j_3 (right ordinate) as a function of k_1. Panel d: E_5 (left ordinate) and compensatory flux j_{11} (right ordinate) as a function of k_1. Rate constants as in Fig 11. Start concentrations (for all 100 data points): A=2.0, E_1=1.63×10^{-6}, and E_5=4.901.

function of the decreasing k_1 values. As in Fig 12 the system shows isolated control, i.e. when M5 actively keeps A at A_{set}^{M5} by compensatory flux j_{11} (with k_1 values between points 1 and 2) the compensatory flux j_3 of M1 is kept low and constant (panel a3). On the other hand, when M1 controls A at A_{set}^{M1} (with k_1 values between points 3 and 4) M5's compensatory flux j_{11} is kept low while M1's compensatory flux j_3 is high and changing with changing k_1/k_2. The border lines in panel a1 are described by Eqs 25-28.

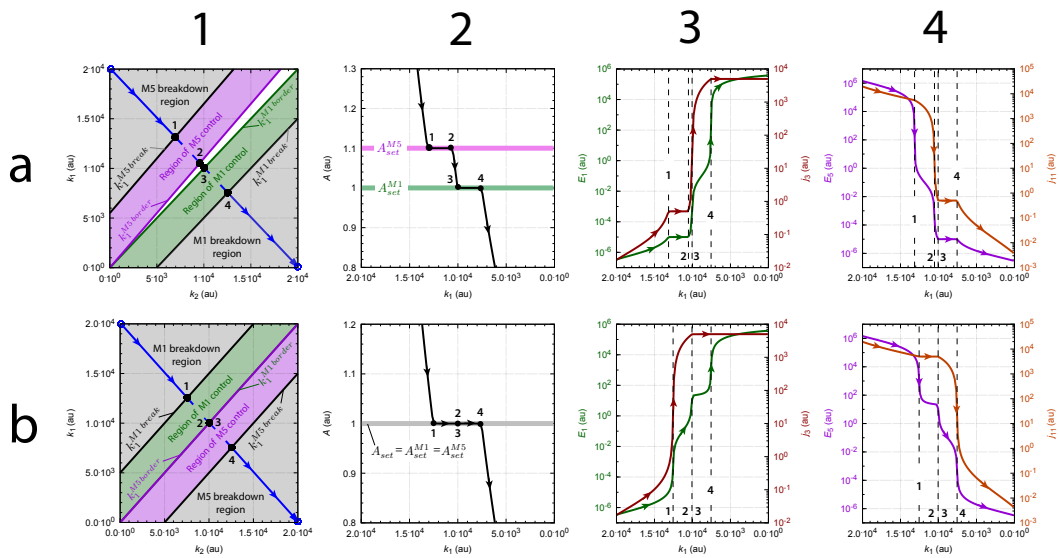

Figure 13: Switch from isolated to delegated control when A_{set}^{M1} and A_{set}^{M5} become equal. Panels a1-a4 show the perturbation phase diagram, A, E_1, j_3, E_5, and j_{11} as a function of k_1 when A_{set}^{M1}=1.0 and A_{set}^{M5}=1.1. The system shows isolated control. Panels b1-b4 show the same system, but now with A_{set}^{M1}=A_{set}^{M5}=1.0. The system has switched to delegated control. Rate constants: k_3=5.0×10^3, k_4=100.0, k_5=100.0, k_6=1.0×10^{-6}, k_7=0.1, k_8=100.0, k_9=110.0 (panels a1-a4), k_9=100.0 (panels b1-b4), k_{10}=1.0×10^{-6}, k_{11}=5.0×10^3, k_{12}=0.1. The blue straight lines in panels a1 and b1 are defined by the following k_1, k_2 values: k_1^{start}=2.0×10^4, k_2^{start}=1.0×10^2 and k_1^{end}=1.0×10^2, k_2^{end}=2.0×10^4. The blue lines were divided into 100 (k_1, k_2) data points. For each point the steady state in A and the other values were determined after 5000 time units. Vertical dashed lines in panels a3-a4 and b3-b4 correspond to the solid dots 1-4, which are the calculated intersection points between the blue line and the border lines Eqs 25-28 (panel a1 for isolated control) and Eqs 19-23 (panel b1 for delegated control). Initial concentrations (panels a1-a4, all 100 data points): A_0=2.0, $E_{1,0}$=1.6315×10^{-6}, and $E_{5,0}$=4.901. Initial concentrations (panels b1-b4, all 100 data points): A_0=3.226, $E_{1,0}$=1.6315×10^{-6}, and $E_{5,0}$=22.26.

By changing k_9 from 110.0 to 100.0 Fig 13 (panels b1-b4) shows the

same system, but now with A_{set}^{M1}=A_{set}^{M5}=1.0: The combined controllers have switched to delegated control. The solid dots in panel b1 represent the calculated intersection points between the straight blue line of the changing k_1's and k_2's and the borderlines of delegated control, i.e. Eqs 19, 20, 22, and 23. Points 2 and 3 have now merged into one point. Panel b2 shows the value of A changing with decreasing k_1. Panel b3 shows the delegated control by M1: While M5 controls A between merged points (2, 3) and 4, M1 submits its entire compensatory flux j_3 to the system (right ordinate). When M1 controls A between points 1 and merged points 2, 3 it is now M5's compensatory flux j_{11} that is high and constant (panel b4, right ordinate). Since A_{set}=A_{set}^{M1}=A_{set}^{M5}=1.0 $k_1^{M1\,border}$ and $k_1^{M5\,border}$ have merged. Furthermore, since k_3=k_{11}=5.0×10^3 we have:

$$k_1^{M1\,border}=k_1^{M5\,border}=A_{set}\cdot(k_2+k_{11})-k_3 \quad \Rightarrow \quad k_1^{M1\,border}=k_1^{M5\,border}=k_2 \qquad (29)$$

3.2.4. Combined M1-M5 controllers with all four activation constants

I further investigated how Michaelis-Menten signaling kinetics from A to E_1 synthesis and from A to E_5 removal would affect the controlled regions of the combined M1 and M5 controllers. For this purpose I used 'mixed activations' as described by Eq 2. Fig 14 shows the updated reaction scheme of the combined M1 and M5 controller with the additional activation constants k_{13} and k_{14}.

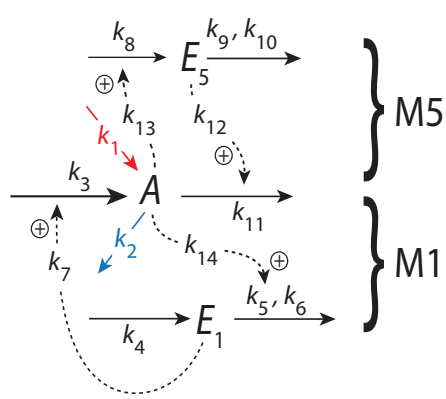

Figure 14: The combined M1-M5 controller with the four activation constants k_7, k_{12}, k_{13}, and k_{14}. M1 and M5 activate their respective compensatory fluxes j_3 and j_{11} via activation constants k_7 and k_{12} (Eq 30). A-induced activations of E_5 synthesis and E_1 removal have the respective activation constants k_{13} and k_{14} (see Eqs 32 and 31).

The rate equations are:

$$\dot{A} = \underbrace{k_1}_{\text{perturbation}} - \underbrace{k_2 \cdot A}_{\text{perturbation}} + \underbrace{k_3 \left(\frac{E_1}{k_7 + E_1} \right)}_{\text{M1 compensatory flux j}_3} - \underbrace{k_{11} \cdot A \left(\frac{E_5}{k_{12} + E_5} \right)}_{\text{M5 compensatory flux j}_{11}} \tag{30}$$

$$\dot{E}_1 = k_4 - k_5 \cdot \underbrace{\left(\frac{E_1}{k_6 + E_1} \right)}_{\approx 1} \cdot \left(\frac{A}{k_{14} + A} \right) \tag{31}$$

$$\dot{E}_5 = k_8 \cdot \left(\frac{A}{k_{13} + A} \right) - k_9 \cdot \underbrace{\left(\frac{E_5}{k_{10} + E_5} \right)}_{\approx 1} \tag{32}$$

Also here integral control is introduced by zero-order kinetic removals of E_1 and E_5 with $E_1/(k_6+E_1) \approx 1$ and $E_5/(k_{10}+E_5) \approx 1$ by using low (1×10^{-6}) k_6 and k_{10} values. From the steady state conditions of Eqs 31 and 32 the setpoints by M1 and M5 are calculated to be:

$$A_{set}^{M1} = k_{14} \left(\frac{k_4}{k_5 - k_4} \right) \tag{33}$$

$$A_{set}^{M5} = k_{13} \left(\frac{k_9}{k_8 - k_9} \right) \tag{34}$$

Fig 15 gives an overview of the combined M1-M5 behaviors when k_{13} and k_{14} are chosen such that A_{set}^{M1}=2.0 and A_{set}^{M5}=1.0 (row a), A_{set}^{M1}=A_{set}^{M5}=2.0 (row b), A_{set}^{M1}=1.0 and A_{set}^{M5}=2.0 (row c). In all three instances the systems' behaviors are calculated along a straight k_1-k_2 line, which starts out at k_1^{start}=2.0×10^4 and k_2^{start}=100.0 and ends at k_1=100.0 and k_2=2.0×10^4. Columns 2-4 show respectively the concentrations of A, E_1 & j_3, and E_5 & j_{11}, as a function of decreasing k_1.

It was found that the system with four activation constants (Eqs 30-32) behaves analogous to the system with only two activation constants (Eqs 13-15). In order words, when $A_{set}^{M1} > A_{set}^{M5}$ (row a, Fig 15) we have 'delegated control' with one controller's compensatory flux fully contributing, while the other controller adjusts its compensatory flux in order to keep A at its setpoint.

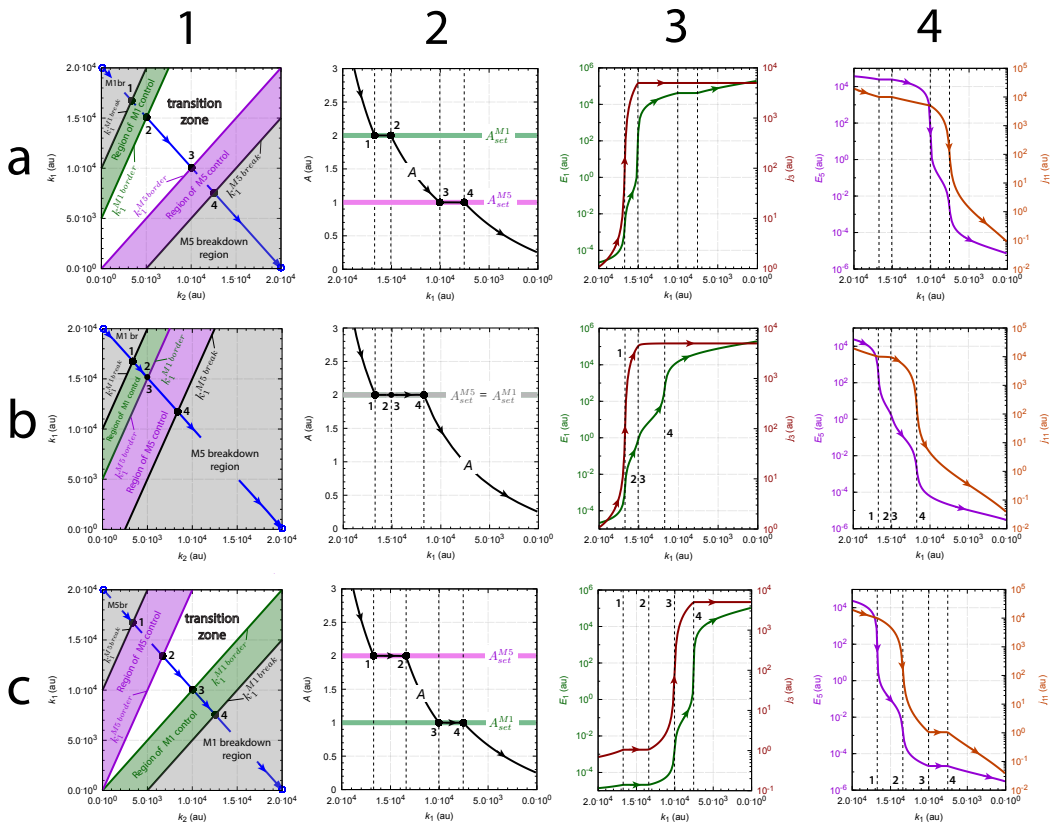

Figure 15: Delegated and isolated control in dependence of three A_{set}^{M1}, A_{set}^{M5} combinations (a-c; Eqs 33-34). In all three instances calculations were performed along a straight line in the perturbation phase diagram (outlined in blue in panels a1, b1, c1) and defined by the blue open circles k_1^{start}=2.0×10^4, k_2^{start}=100.0, and k_1^{end}=100, k_2^{end}=2.0×10^4. The line was divided into 100 data points and for each k_1, k_2 set A, E_1, E_5 and the respective compensatory fluxes j_3 and j_{11} were determined after 5000 time units. Columns 2-4 show the values of A, E_1, E_5 and the corresponding compensatory fluxes j_3 and j_{11}. Row a: A_{set}^{M1}=2.0 and A_{set}^{M5}=1.0 by k_{13}=0.05, and k_{14}=0.2. Row b: A_{set}^{M1}=2.0 and A_{set}^{M5}=2.0 by k_{13}=0.1, and k_{14}=0.2. Row c: A_{set}^{M1}=1.0 and A_{set}^{M5}=2.0 by k_{13}=0.1, and k_{14}=0.1. Rate constants: k_3=5.0×10^3, k_4=100.0, k_5=110.0, k_6=1.0×10^{-6}, k_7=0.1, k_8=210.0, k_9=200.0, k_{10}=1.0×10^{-6}, k_{11}=5.0×10^3, k_{12}=0.1. Initial concentrations (for all calculations): A_0=2.0, $E_{1,0}$=2.1×10^{-5}, $E_{5,0}$=0.1.

When A_{set}^{M1}=A_{set}^{M5} (row b, Fig 15) both controllers cooperate in their actions, i.e. while one controller (here M1) increases its compensatory flux j_3 when moving along the blue line in panel b1, the other controller (M5) decreases its compensatory flux j_{11}. When finally j_3 reaches its maximum

(panel b3) M5 controls A by further decreasing its compensatory flux (panel b4): the system shows 'delegated control'.

When $A_{set}^{M1}<A_{set}^{M5}$ (row c, Fig 15) the system shows 'isolated control'. Here, during control of A by M5 (between points 1 and 2), the compensatory flux of M1 (j_3) is low and constant (panel c3) and does not significantly contribute to the control of A. The situation is reversed when A is controlled by M1: now M5's compensatory flux (j_{11}) is constant and negligible (panel c4).

In summary, although the introduction of the activation constants k_{13} and k_{14} affect the values of the M1 and M5 setpoints, the borderlines for delegated and isolated control are still described by respectively Eqs 19, 20, 22, and 23 and Eqs 25, 26, 27, and 28. In fact, the two sets of borderlines for delegated and isolated control remain the same also for the other controller combinations (see `Sup1.pdf`). The videos `Sup4.mp4`-`Sup7.mp4` illustrate how the control regions of the inflow and outflow controllers are affected during delegated and isolated control when rate constants k_3 or k_{11} of the compensatory fluxes change.

3.2.5. Compensatory first-order kinetics with respect to E_1 and E_5 leads to extended control regions

It is further found that the reaction order with respect to the controller variables affect the regions of control significantly. In the following example the compensatory fluxes of M1 and M5 are first-order with respect to E_1 and E_5 changing A's rate equation to

$$\dot{A} = \underbrace{k_1 - k_2 \cdot A}_{\text{perturbations}} + \underbrace{k_3 \cdot E_1}_{\text{M1 compensatory flux j}_3} - \underbrace{k_{11} \cdot A \cdot E_5}_{\text{M5 compensatory flux j}_{11}} \tag{35}$$

while the rate equations of E_1 and E_5 remain the same (Eqs 14 and 15). Enzyme-catalyzed reactions can show first-order (or close to first-order) kinetics during low-affinity binding between enzyme and substrate, i.e. when the K_M becomes much larger than an enzyme's substrate concentration, i.e. when $v{=}V_{max}{\cdot}S/(K_M{+}S) \approx (V_{max}/K_M){\cdot}S$.

Fig 16 shows a calculation with the same parameters as in Fig 12 except that the rate equation of A, Eq 13, has been replaced by Eq 35. As the saturations in j_3 and j_{11} are now missing the M1 and M5 control of A can extend along the k_1 and k_2 axes as long as no limits on the growth of E_1

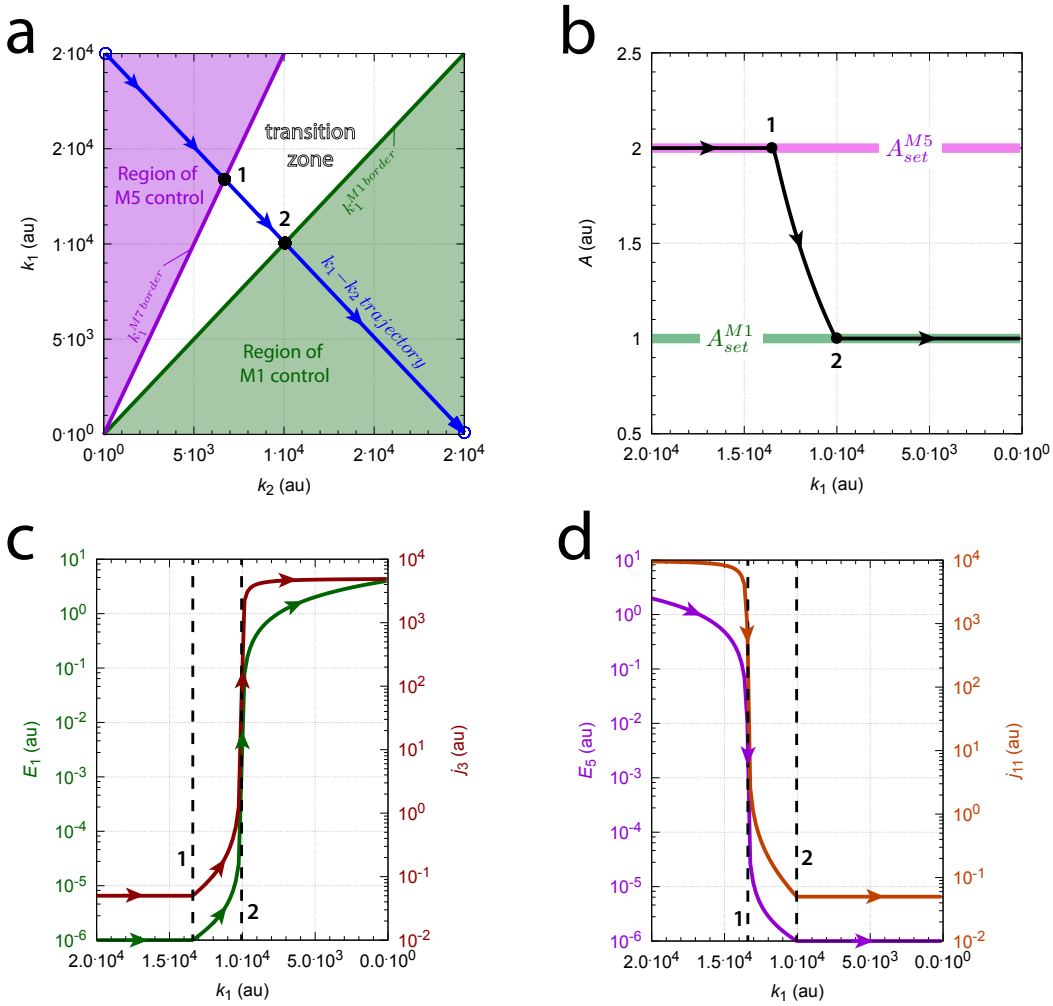

Figure 16: Extended regions of M1 and M5 control by first-order compensatory fluxes with respect to M1 and M4 (Eq 35). Rate parameters and initial concentrations as in Fig 12.

and E_5 are encountered. Clearly, this is a highly idealized situation, but could occur in a biological system by different E_1 and E_5 species which are successively expressed when there is a need for an increased compensatory flux with lower affinity regulation. An analogous regulation is well-known to occur for low- or high affinity transport processes (Huang et al., 2011; Bosdriesz et al., 2018).

3.3. The combined controllers' windup behaviors

In Fig 9 (and Figs S9 and S14, `Sup2.pdf`) it is shown that positive windup leads to very long settling times. On the other hand, when windups are negative settling times are short (Fig 11 and Figs S11, S16 in `Sup2.pdf`). Table 1 gives an overview of the positive and negative windup behaviors when controller combinations show delegated or isolated control. Controller combinations showing negative windup (both $\dot{E}_{inflow}$ and $\dot{E}_{outflow}$ are negative) are outlined in blue, while controller combinations with positive windup (both $\dot{E}_{inflow}$ and $\dot{E}_{outflow}$ are positive) are outlined in red. Controller combinations with mixed positive and negatived windups are indicated in yellow.

Table 1: Overview of combined controllers' windup behaviors

Controllers	$A_{set}^{inflow} > A_{set}^{outflow}$ delegated control	$A_{set}^{inflow} < A_{set}^{outflow}$ isolated control
M1-M5	$\dot{E}_1 > 0,\ \dot{E}_5 > 0$	$\dot{E}_1 < 0,\ \dot{E}_5 < 0$
M1-M6	$\dot{E}_1>0,\ \dot{E}_6<0$	$\dot{E}_1<0,\ \dot{E}_6>0$
M1-M7	$\dot{E}_1>0,\ \dot{E}_7>0$	$\dot{E}_1<0,\ \dot{E}_7<0$
M1-M8	$\dot{E}_1>0,\ \dot{E}_8<0$	$\dot{E}_1<0,\ \dot{E}_8>0$
M2-M5	$\dot{E}_2<0,\ \dot{E}_5>0$	$\dot{E}_2>0,\ \dot{E}_5<0$
M2-M6	$\dot{E}_2<0,\ \dot{E}_6<0$	$\dot{E}_2>0,\ \dot{E}_6>0$
M2-M7	$\dot{E}_2<0,\ \dot{E}_7>0$	$\dot{E}_2>0,\ \dot{E}_7<0$
M2-M8	$\dot{E}_2<0,\ \dot{E}_8<0$	$\dot{E}_2>0,\ \dot{E}_8>0$
M3-M5	$\dot{E}_3>0,\ \dot{E}_5>0$	$\dot{E}_3<0,\ \dot{E}_5<0$
M3-M6	$\dot{E}_3>0,\ \dot{E}_6<0$	$\dot{E}_3<0,\ \dot{E}_6>0$
M3-M7	$\dot{E}_3>0,\ \dot{E}_7>0$	$\dot{E}_3<0,\ \dot{E}_7<0$
M3-M8	$\dot{E}_3>0,\ \dot{E}_8<0$	$\dot{E}_3<0,\ \dot{E}_8>0$
M4-M5	$\dot{E}_4<0,\ \dot{E}_5>0$	$\dot{E}_4>0,\ \dot{E}_5<0$
M4-M6	$\dot{E}_4<0,\ \dot{E}_6<0$	$\dot{E}_4>0,\ \dot{E}_6>0$
M4-M7	$\dot{E}_4<0,\ \dot{E}_7>0$	$\dot{E}_4>0,\ \dot{E}_7<0$
M4-M8	$\dot{E}_4<0,\ \dot{E}_8<0$	$\dot{E}_4>0,\ \dot{E}_8>0$

Since the results above indicate that the eight delegated and isolated control modes outlined in blue are expected to be more rapid in their switching/settling between and within control regions, and also more economic by avoiding time- and energy requiring windups, one might speculate whether

these controller combinations may be more frequently represented in nature; required that control is mediated between flatly combined inflow and outflow controllers as considered here. The isolated control mode of the M3-M5 controller will be used below to describe blood glucose homeostasis.

3.4. Metastability

The term 'metastability' or 'metastable control' refers to the observation that in certain cases one of the controllers can temporarily gain control over A when one of the controller variables (the E_i's) are suddenly added or removed. Fig 17 shows an example with the combined M1-M5 controller (Fig 8): By adding 1000 units of E_1 to the system M5's isolated control of A at A_{set}^{M5}=2.0 is turned into a temporary control by M1 at A_{set}^{M1}=1.0. Panel a shows the system's perturbation phase diagram with the k_1 and k_2 parameters indicated as a dot. Panel b shows the A behavior: Right after the E_1 addition A goes into a steady state (induction period) as j_3 is driven to its maximum k_3, while E_1 decreases (panel c). While j_3 is at its maximum E_5 increases, but its compensatory flux j_{11} is -like j_3- fully saturated (panel d), i.e. for both M5 and M1 we have $E_5/(k_{12}+E_5)\approx 1$ and $E_1/(k_7+E_1)\approx 1$. The A-steady state can be determined form the rate equation of A:

$$\dot{A} = k_1 - k_2 \cdot A_{ss} + k_3 - k_{11} \cdot A_{ss} = 0 \;\; \Rightarrow \;\; A_{ss} = \frac{k_1 + k_3}{k_2 + k_{11}} \tag{36}$$

When E_1 has reached its minimum again the growth in E_5 stops and E_5 starts to decrease. It is during the E_5 decrease that the metastable M1 state appears (panel b). When E_5 has reached its minimum A_{ss} returns to A_{set}^{M5}.

Fig 18 shows the induction of the metastable M1 state by adding 1000 E_5 units instead of adding E_1, otherwise the system is the same as in Fig 17 (panel a). Here, the induction period characterized by $A_{ss}=(k_1+k_3)/(k_2+k_{11})$ is missing prior to the appearing metastable M1 state (panel b). Instead, E_1 and j_3 go rapidly into steady states (panel c), while E_5 is immediately driven to a maximum level and starts to decrease (panel d). As in Fig 17 it is during the decrease of E_5 M1 metastability is observed (panel b).

There is also the peculiar case when the metastable state has the same setpoint as the original stable one. Figs 19 and 20 show two examples. In Figs 19 we start out with a stable M1 state indicated by the dot in panel a. When 1000 E_1 units are added the same sequence of events occur as in Fig 16: directly after the E_1 addition A goes into a steady state characterized by $A_{ss}=(k_1+k_3)/(k_2+k_{11})$ (panel b) while E_1 is decreasing and M2's

compensatory flux is at its maximum j_3=k_3 (panel c). During this period E_5 increases (panel d). Once E_1 has reached a minimum value j_3 and j_{11} go into a new steady state and E_5 starts to decrease. During the E_5 decrease M1 is metastable (panels b and d). When E_5 has reached its minimum value the end of the metastable state is indicated by a spike of A and the system returns to its original state.

Fig 20 starts out with the same M1 state as in Fig 19, but 1000 E_5 units are added instead. The sequence of events is the same as in Fig 18: directly after the E_5 addition A goes into the M1 metastable state (panel b) while E_1 and j_3 are in steady states (panel c). During the metastable M1 state E_5 decreases until it reaches its minimum value and the end of the metastable state (panel d). The beginning and the end of the M1 metastable state are characterized by the negative and positive A-spikes (panel b).

In supporting material Sup3.pdf additional examples of metastability are given due to windup or by adding/removing a controller variable.
Concerning the question when metastability can be expected to occur or not, reference is made to Table 1. Loosely speaking, for all controller variables with positive windup no metastability is expected to occur by adding the windup species, since the addition of a controller variable does in this case not change the corresponding compensatory flux, which may already be saturated. Likewise for negative windups and removals, as removal of a controller variable already low is expected not to affect the steady state of A. Only during negative windup additions may lead to metastability as the four examples above for the isolated M1-M5 controller indicate. There, where the controller variable undergoes positive windup removal of this variable may temporarily drive A into the control domain of the other (antagonistic) controller. See for example Fig S3, panels a3 and b3 in Sup3.pdf. However, to predict the occurrence of a metastable state appears difficult since metastability is dependent on rate parameters and the relative positions of setpoints as shown in Sup3.pdf.

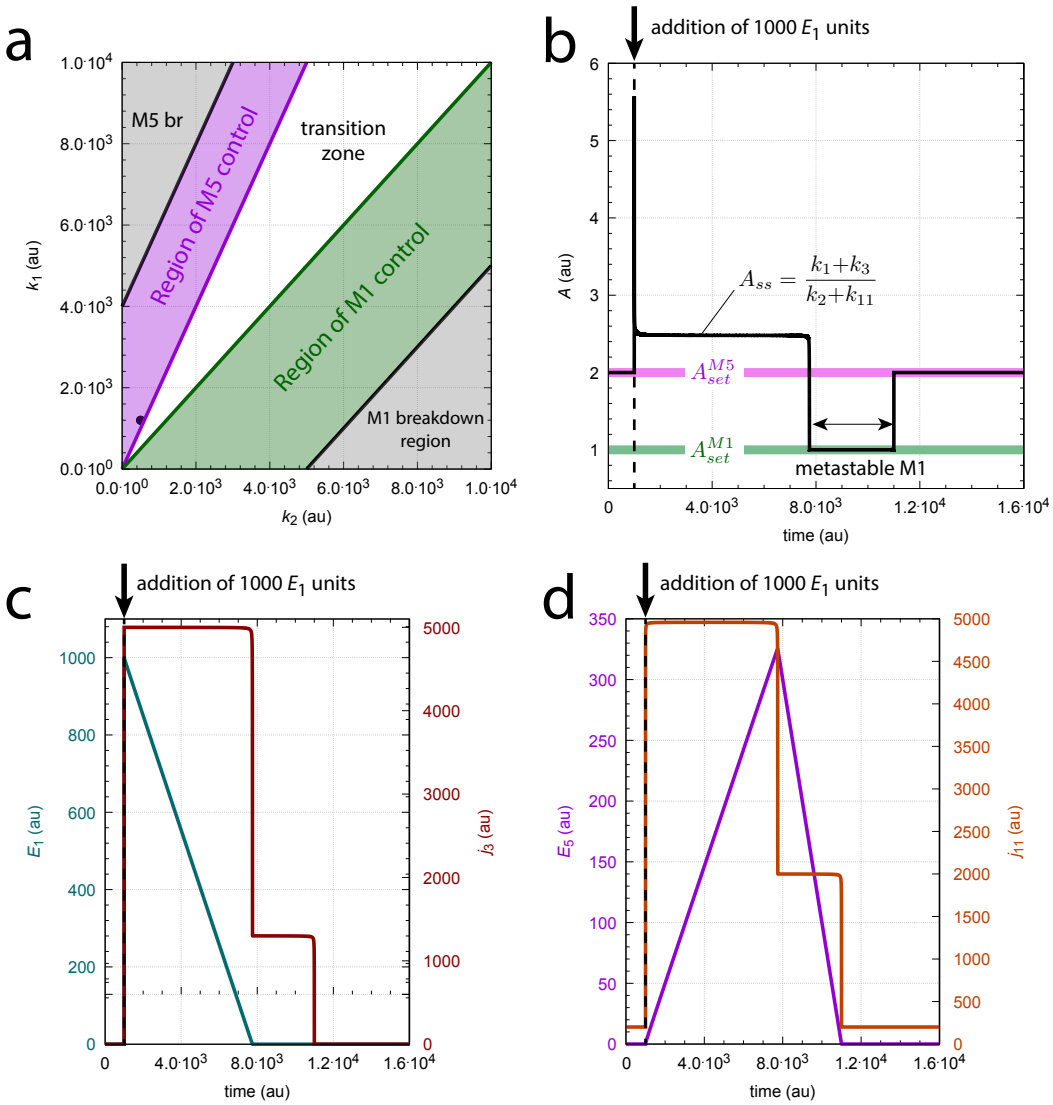

Figure 17: Metastable M1 control by adding E_1 to isolated M5 control. Panel a: Perturbation phase diagram. The dot indicates the values k_1=1.2×10^3 and k_2=5.0×10^2. Panel b: A as a function of time. The metastable M1 region is indicated by the double-arrow. Panel c: E_1 (left ordinate) and M2's compensatory flux j_3 (right ordinate) as a function of time. Panel d: E_5 (left ordinate) and M5's compensatory flux j_{11} (right ordinate) as a function of time. Vertical arrows indicate the addition of 1000 E_1 units at t=1000.0. Other rate constants: k_3=5.0×10^3, k_4=0.1, k_5=0.1, k_6=1.0×10^{-6}, k_7=0.1, k_8=0.1, k_9=0.2, k_{10}=1.0×10^{-6}, k_{11}=2.0×10^3, k_{12}=0.1. Initial concentrations: A_0=2.0, $E_{1,0}$=1.0×10^{-6}, and $E_{5,0}$=5.27×10^{-3}.

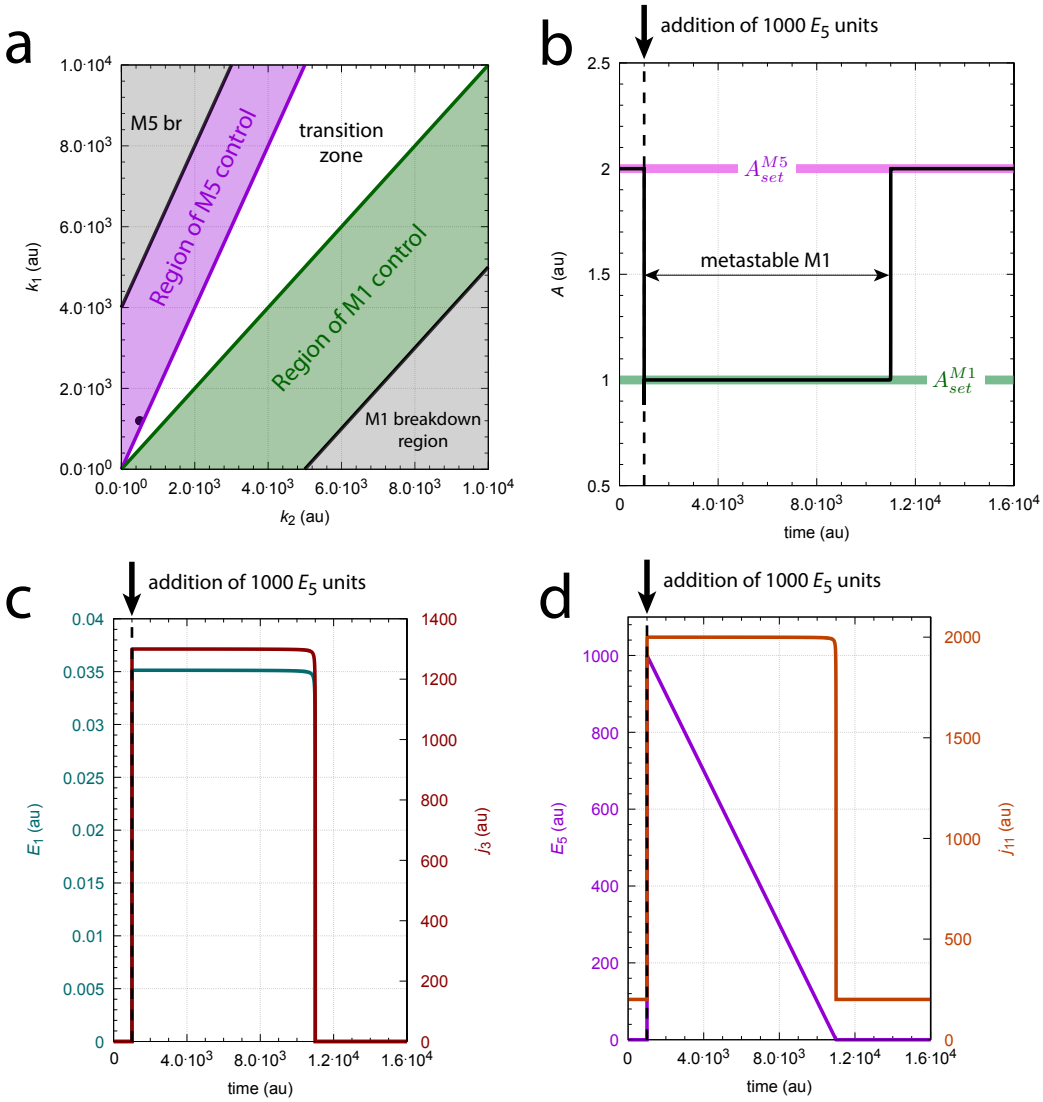

Figure 18: M1 metastability induced by adding E_5 at isolated M5 control. Panel a: Perturbation phase diagram. The dot indicates the values k_1=1.2×10^3 and k_2=5.0×10^2. Panel b: A as a function of time. The metastable M1 region is indicated by the double-arrow. Panel c: E_1 (left ordinate) and M2's compensatory flux j_3 (right ordinate) as a function of time. Panel d: E_5 (left ordinate) and M5's compensatory flux j_{11} (right ordinate) as a function of time. Vertical arrows indicate the addition of 1000 E_5 units at t=1000.0. Other rate constants as in Fig 17.

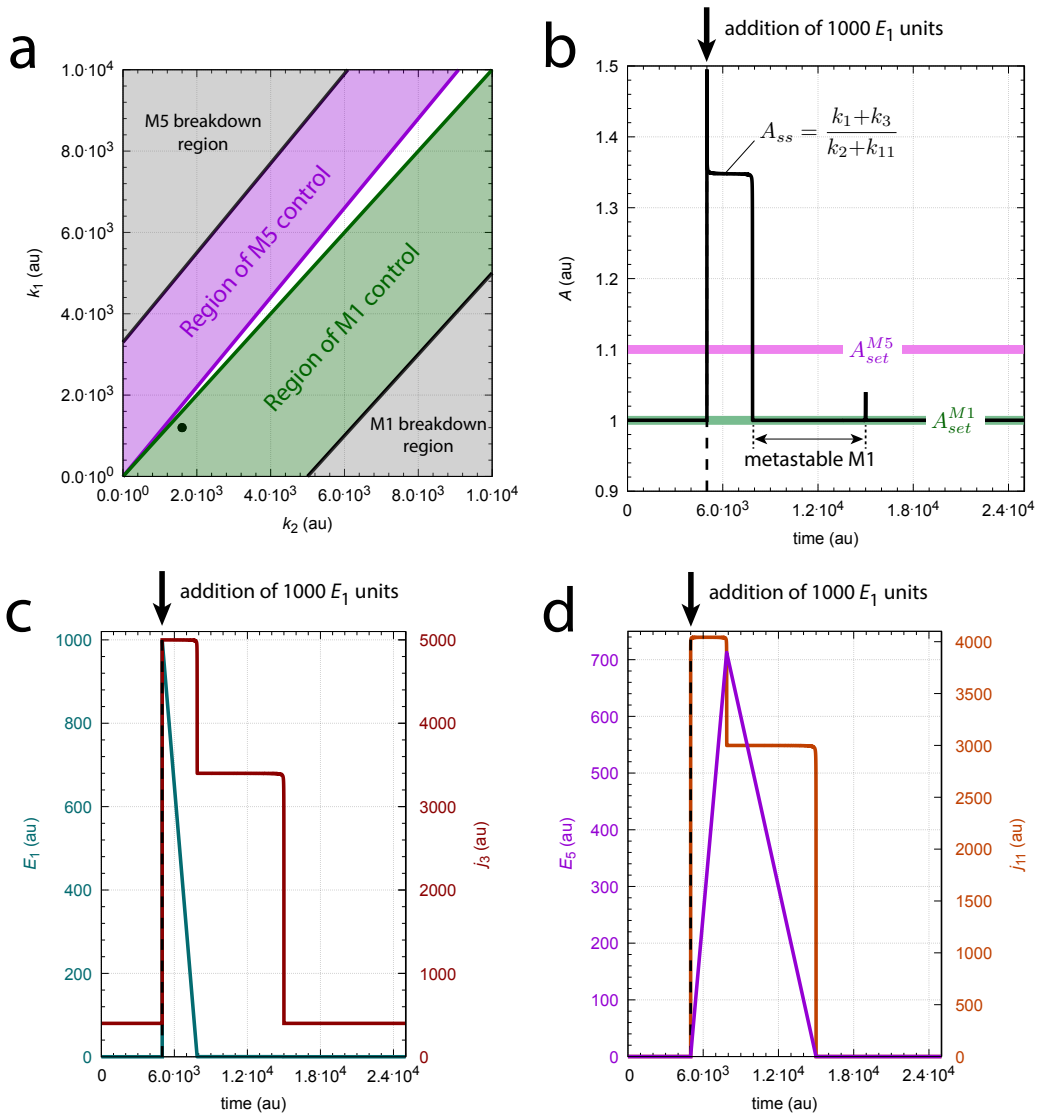

Figure 19: Transition between a M1 stable and a M1 metastable state by adding E_1. Panel a: Perturbation phase diagram. The dot indicates the perturbations k_1=1200 and k_2=1600. Panel b: A levels as a function of time. Panel c: E_1 (left ordinate) and M2's compensatory flux j_3 (right ordinate) as a function of time. Panel d: E_5 (left ordinate) and M5's compensatory flux j_{11} (right ordinate) as a function of time. Vertical arrows indicate the addition of 1000 E_1 units at t=5000.0. Other rate constants: k_3=5.0×10^3, k_4=1.0, k_5=1.0, k_6=1.0×10^{-6}, k_7=0.1, k_8=1.0, k_9=1.1, k_{10}=1.0×10^{-6}, k_{11}=3.0×10^3, k_{12}=0.1. Initial concentrations: A_0=1.0, $E_{1,0}$=8.71×10^{-3}, and $E_{5,0}$=1.0×10^{-5}.

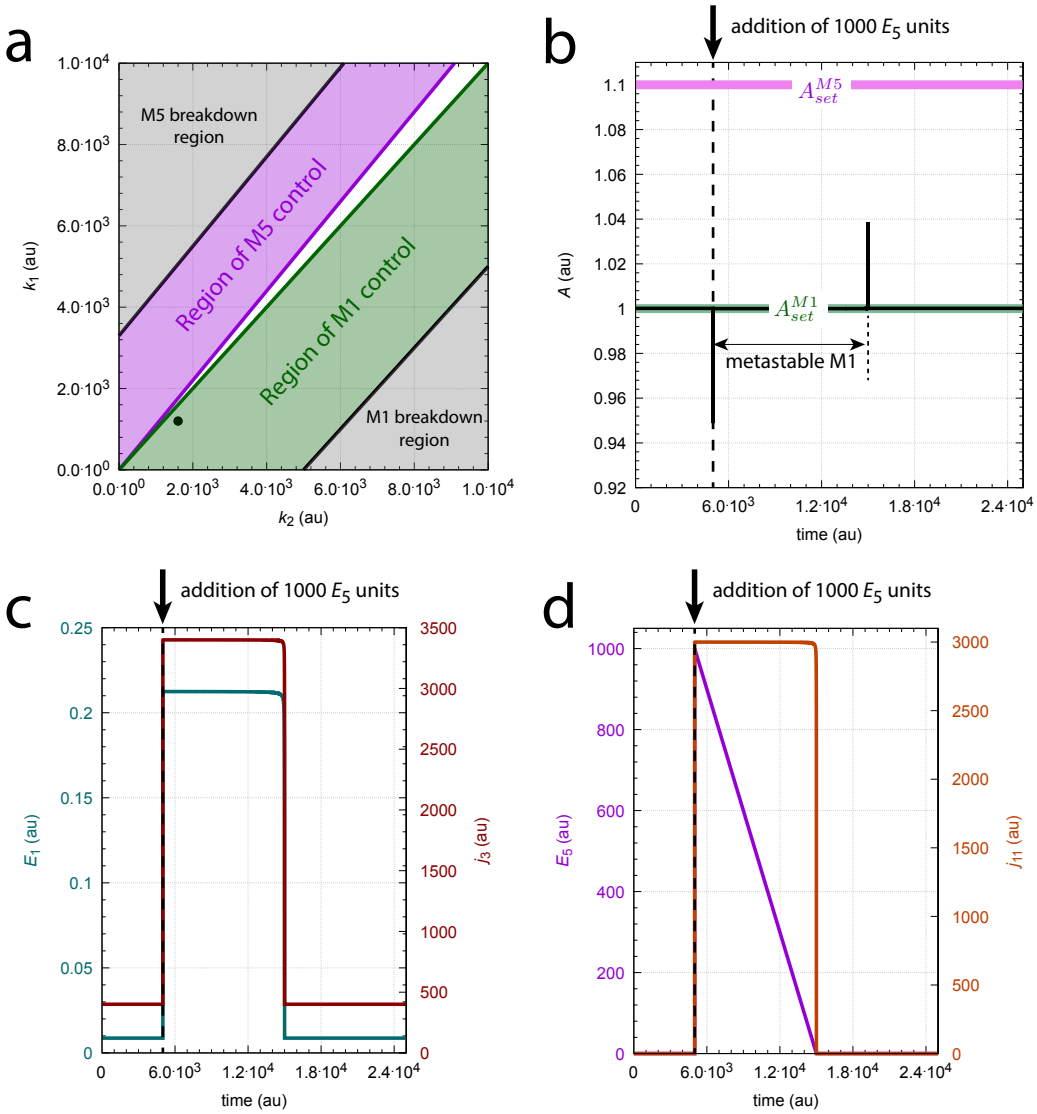

Figure 20: Transition between a M1 stable and a M1 metastable state by addition of E_5. Panel a: Perturbation phase diagram. The dot indicates the perturbations k_1=1200 and k_2=1600. Panel b: A levels as a function of time. Panel c: E_1 (left ordinate) and M2's compensatory flux j_3 (right ordinate) as a function of time. Panel d: E_5 (left ordinate) and M5's compensatory flux j_{11} (right ordinate) as a function of time. Vertical arrows indicate the addition of 1000 E_1 units at t=5000.0. Rate constants and initial concentrations as in Fig 19.

3.4.1. Perfect adaptation without integral feedback

Robust perfect adaptation is closely associated with integral control. However, there are examples where perfect or near-perfect adaptation can occur in an open loop setting or by high and constant controller variables. I will use the combined M1-M5 controller as an illustration.

When, under delegated control, the compensatory fluxes j_3 and j_{11} (Eq 13) are replaced by first-order expressions with respect to E_1 and E_5 (i.e. having low affinity compensatory fluxes), such that

$$j_3 = k_3 \cdot E_1 \tag{37}$$

and

$$j_{11} = k_{11} \cdot A \cdot E_5 \tag{38}$$

M1 and M5 work against each other and both E_1 and E_5 show linear integral windup as discussed in the supporting material by Drengstig et al. (2012a) (Fig S15, page 22ff). However, what was not realized at that time is that A in fact shows robust perfect adaptation. The setpoint

$$A_{set} = \frac{k_1 + k_3 \cdot E_1}{k_2 + k_{11} \cdot E_5} \;\rightarrow\; \frac{k_3 \cdot E_1}{k_{11} \cdot E_5} \;\rightarrow\; \frac{k_3 \cdot \dot{E}_1}{k_{11} \cdot \dot{E}_5} \tag{39}$$

can be obtained by substituting Eqs 37 and 38 into Eq 13 and solving for A. The ratio after the first arrow in Eq 39 is a result of the linear increases of E_1 and E_5 such that the k_1 and k_2 terms eventually can be neglected. The ratio after the second arrow is due to the fact that E_1 and E_5 increase linearly with time. As $\dot{E}_1$ and $\dot{E}_5$ also depend on k_4, k_5, k_8, and k_9 A_{set} will in addition be implicitly determined by these parameters. Thus, the steady state of A will eventually reach A_{set} defined by

$$A_{set} = \frac{k_3 \cdot \dot{E}_1}{k_{11} \cdot \dot{E}_5} \tag{40}$$

Fig 21 illustrates the behavior by using the k_1/k_2 values from Fig 9. The rate constants used give a A_{set} of precisely 2.0. A typical property of this type of robust control is that the k_1/k_2-induced A excursions diminish as E_1 and E_2 grow.

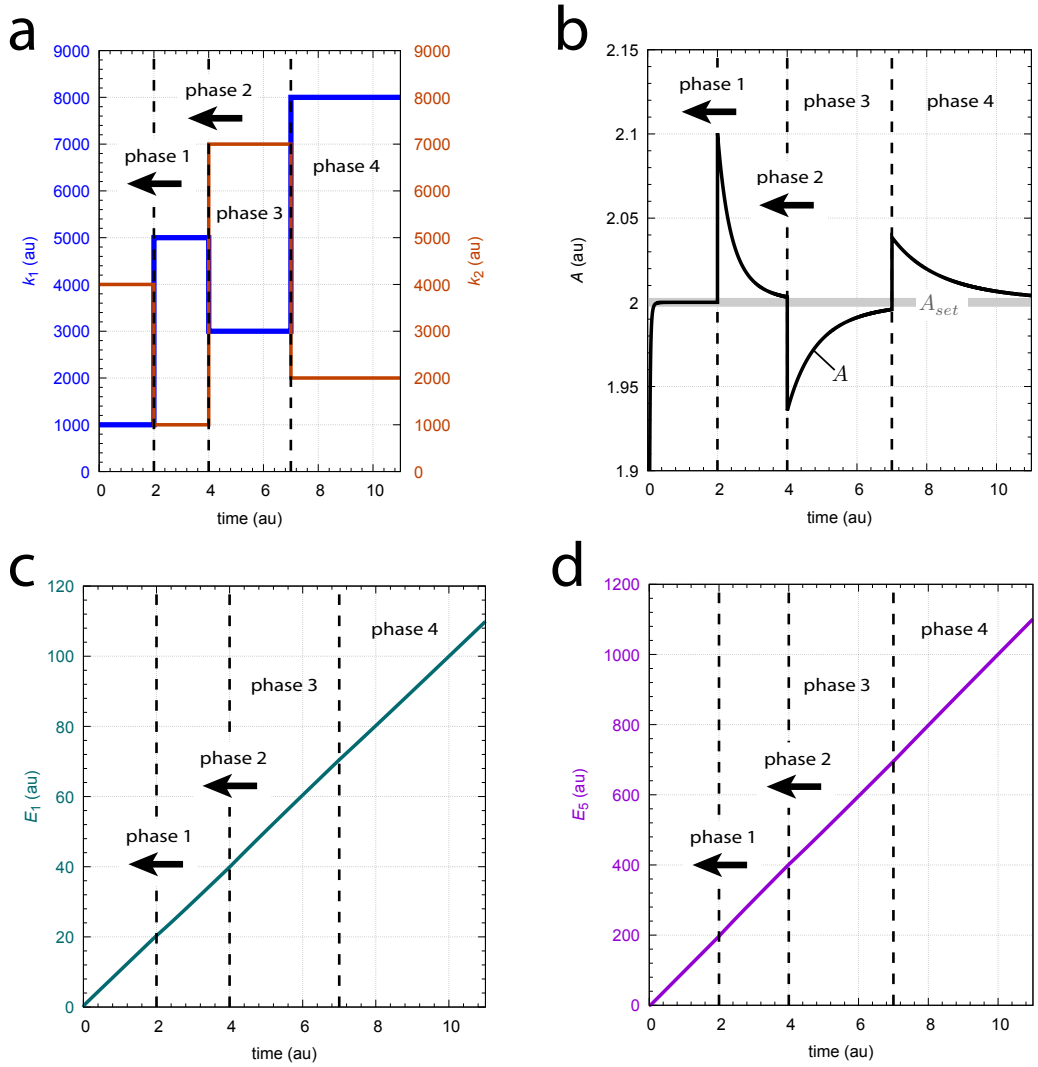

Figure 21: Robust perfect adaptation when $A_{set}^{M1}>A_{set}^{M5}$ and compensatory fluxes follow first-order kinetics by Eqs 37 and 38. Panel a: k_1 and k_2 as a function of time. Phase 1: k_1=1.0×10^3, k_1=4.0×10^3; phase 2: k_1=5.0×10^3, k_1=1.0×10^3; phase 3: k_1=3.0×10^3, k_1=7.0×10^3; phase 4: k_1=8.0×10^3, k_1=2.0×10^3. Panel b: A as a function of time. Panels c and d show the linear increase of respectively E_1 and E_5. Rate constants: k_3=1.0×10^4, k_4=30.0, k_5=10.0, k_6=1.0×10^{-6}, k_7 not used, k_8=100.0, k_9=100.0, k_{10}=1.0×10^{-6}, k_{11}=50.0, k_{12} not used. Initial concentrations: A_0=$E_{1,0}$=$E_{5,0}$=0.0. See Python code for details.

Since the M1 and M5 feedback structures in Fig 21 are broken due to the

windup of E_1 and E_5 Fig 22 shows an analogous mechanism for robust perfect adaptation without being based on integral feedback. The rate equations are in this case:

$$\dot{A} = k_1 - k_2 \cdot A + k_3 \cdot E_1 - k_{11} \cdot A \cdot E_5 \tag{41}$$

$$\dot{E}_1 = k_4 \tag{42}$$

$$\dot{E}_5 = k_8 \tag{43}$$

with the setpoint described by Eq 40. It may be mentioned that there occurs no 'breakdown' with respect to k_1 and k_2 perturbations as long as Eqs 41-43 are obeyed.

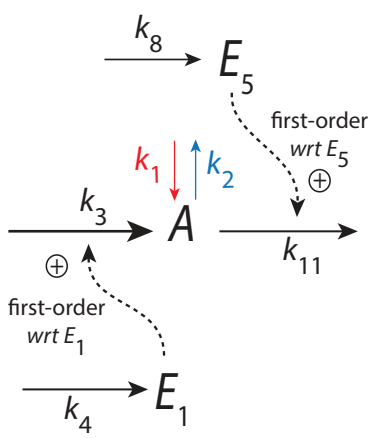

Figure 22: A mechanism for robust perfect adaptation without integral feedback. The mechanism is based on zero-order synthesis rates of E_1 and E_5 and first-order compensatory fluxes with respect to E_1 and E_5. For rate equations see Eqs 41-43.

3.4.2. Compensatory first-order kinetics with large constant E_1 and E_5 leads to near perfect adaptation

The growth of the controller species (here E_1 and E_5) during windup cannot continue indefinitely in a physiological system. At some point resources to build E_1 and E_5 come to a limit. A possible scenario to maintain near perfect homeostasis (as this seem to occur in biological systems) is that E_1 and E_5 are kept at a constant steady-state, but that E_1, E_5 concentrations are such high that A can be kept near an unperturbed reference value (A_{ref})

when k_1=0.0 and k_2=0.0. In other words, A_{ss} can be described during k_1,k_2 perturbations by Eq 39. Note that A does not approach a setpoint, but is kept close to A_{ref}, i.e.

$$A_{ss} = \frac{k_1 + k_3 \cdot E_1}{k_2 + k_{11} \cdot E_5} \approx \frac{k_3 \cdot E_1}{k_{11} \cdot E_5} = A_{ref} \tag{44}$$

Fig 23 shows a calculation with the same perturbations and rate constants as in Fig 21, but with E_1 and E_5 kept constant at respectively 1×10^3 and 1×10^5 leading to A_{ref}=2.0. As this type of regulation can keep A within certain limits (of course, dependent on evolutionary anticipated k_1 and k_2 perturbation ranges) one may wonder to what extent such an approach may be used in physiology.

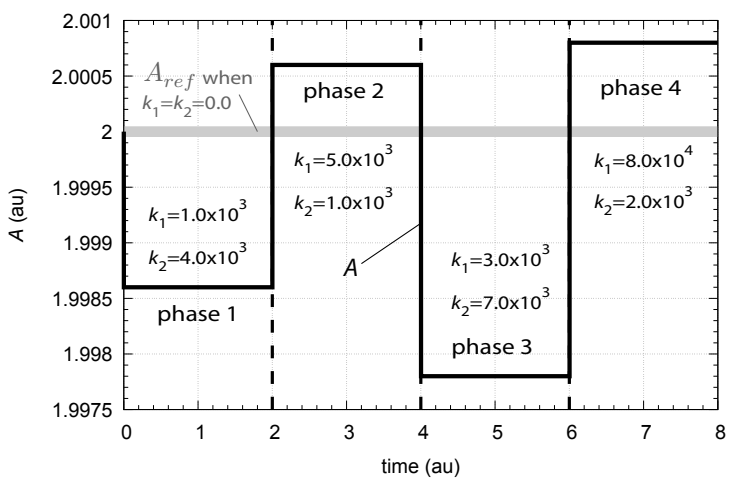

Figure 23: Constant E_1 and E_5 concentration can keep A levels relatively close to A_{ref} (Eq 44). Perturbations and rate constants k_3 and k_{11} as in Fig 21. Constancy of E_1 and E_{11} is achieved by setting in the calculations $\dot{E}_1$ and $\dot{E}_5$ to zero. Initial concentrations: A_0=2.0, $E_{1,0}$=1×10^3, and $E_{5,0}$=1×10^5. See Python code for details.

4. Discussion: Two biological examples

Physiological regulations are extremely complex and the above described models will certainly lack many properties in an organism or cellular-wide regulatory setting. Still, two-setpoint models can provide essential regulatory behaviors as the two examples will demonstrate.

One of the distinctive properties of the above described controllers is the change of the controlled variable between the controllers' two setpoints when environmental conditions cause a sweep across the perturbation phase diagram. A striking example of such behavior is the photoperiodic change of the Siberian hamster's body weight.
The other example relates to blood glucose homeostasis. Although the major drivers of blood glucose regulation (i.e., insulin, glucagon, and somatostatin) are well established, there is still a debate about what determines the glycemic setpoint (Huang et al., 2024). Addressing this debate, a two-setpoint model is put forward to show how such a model in a straightforward way can describe several aspects of intact and diabetic blood glucose regulation.

4.1. Rheostasis by two-setpoint models: The Siberian hamster's photoperiodic changes of body weight

An illustrative case of rheostasis, for example in comparison with Fig 16b, is the seasonal change of the Siberian hamster's body weight. The white data points in Fig 24 show the average reference weight when hamsters were kept at summer day-night changes (16 hours light and 8 hours darkness). At week 0 hamsters were transferred to a winter light-dark regime (8 hours light and 16 hours darkness). Although food supply was not limited weights decreased and approached a new but lower level. Both the summer and the winter weights were found to be under homeostatic control. Although we do not know how k_1 and k_2 in Fig 16b relate to the hamster's body weight it appears that weight changes during summer and winter periods are due to photoperiodic-induced regulations of the hamster's food intake and consumption controlled via the hypothalamus (Bao et al., 2019).

The data in Fig 24 have been interpreted (Stevenson, 2024) to be due to rheostatic control, which includes an apparent change in setpoint. There is the claim (Mrosovsky, 1990; Stevenson, 2024) that homeostatic and rheostatic control are fundamentally different. Among the differences it has been postulated that rheostatic systems lack a defined setpoint. Although this may be possible, the combined M1-M5 controller of Fig 16b and the other examples above show that analogous behaviors to Fig 24 can indeed be described by homeostatic mechanisms with defined setpoints.

Concerning the physiological regulation of the Siberian hamster's body weights, the two negative feedbacks which appear to be involved relate to

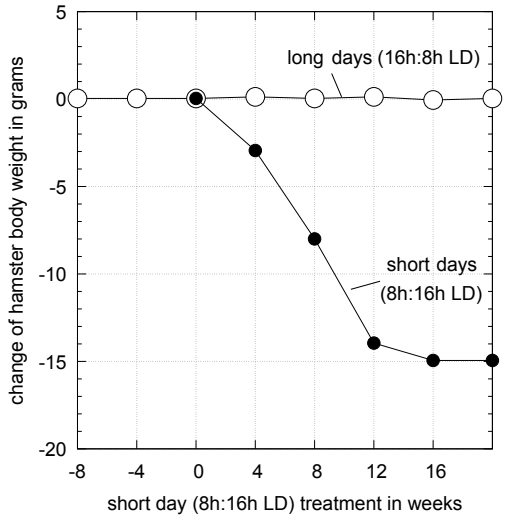

Figure 24: Photoperiod induced changes of the Siberian hamster's body weight. White dots show the control when hamsters are kept at a summer 16h:8h light:dark (LD) regime. Black dots show the loss of body weight when hamsters were transferred to winter 8h:16h LD changes. Both summer and winter weights were found to be under homeostatic control. Redrawn from Stevenson (2024), Fig. 2.4.

two tissue-dependent circadian oscillators. They were identified in hamsters' superchiasmatic nucleus (which is part of the hypothalamus) as morning (M) and evening (E) oscillators (Jagota et al., 2000), after postulating them by Pittendrigh and Daan (1976). Circadian oscillations are based on transcriptional-translational negative feedback loops (Dunlap, 1999), which have homeostatic properties (Saito et al., 2025) and show temperature compensation (Rensing et al., 1997). The circadian organization into two antagonistic negative feedbacks seems to be a general regulatory feature and has been found also in other organisms, ranging from protists (Morse et al., 1994) to fungi (De Paula et al., 2007), insects (Stoleru et al., 2007), and mammals (Helfrich-Förster, 2009). The body weight regulation in hamsters have been found to occur via melatonin, an important transducer of photoperiodic signals. Changes in hamsters body weight can in fact be mimicked by systemic administrations of melatonin (Bartness and Wade, 1985). By studying the enzyme arylalkylamine N-acetylytansferase (NAT), which takes part in the synthesis of melatonin, Illnerová (1991) concluded that there is strong support that NAT rhythmicity and melatonin production is due to the dual E-M

negative feedback structure proposed by Pittendrigh and Daan. In this respect, A would refer to melatonin which determines hamster body weight while the perturbations would relate to the applied photoperiod. While our above two-feedback approach is clearly oversimplified with respect to hamster physiology, it would nevertheless be interesting to pursue this line of research under oscillatory circadian conditions.

Arguments brought forward against a homeostatic interpretation of rheostatic behaviors have implicitly assumed that homeostasis occurs only by single negative feedback loops (see for example chapter 1 in Mrosovsky (1990)). However, such an assumption has never been part of Cannon's definition of homeostasis. In the definition chapter of his 1929 paper Cannon writes (page 251): *The coordinated physiological reactions which maintain most of the steady states in the body are so complex, and are so peculiar to the living organism, that it has been suggested Cannon (1926)* [see a facsimile of this citation in Langley (1973)] *that a specific destination for these states be employed–homeostasis.*

'Rheostasis' as a descriptive term to indicate apparent changes in a setpoint (or using the term *enantiostasis* (Mangum and Towle, 1977; Hochachka and Somero, 1984) to describe a preserved functional relationship with respect to environmental changes) is useful, but the declaration that the underlying control mechanisms of rheostasis are devoid of setpoints and of homeostatic mechanisms, (see description of Fig 2.5 in Stevenson (2024)), appears too dogmatic.

4.2. Blood sugar homeostasis: Predictions by a two-setpoint model

Insulin, glucagon and somatostatin are the major regulators of blood sugar homeostasis. They are produced by different cell types contained in the islets of Langerhans (Clancy and McVicar, 2002; Kumar et al., 2013). Beta cells produce insulin, which, among other roles, enables the entrance of glucose into cells to generate energy.

In this respect, insulin is part of an *outflow controller* which reduces the amount of blood sugar. Alpha cells produce glucagon, which have an glycogenolytic activity, i.e. glucagon increases blood glucose from stored glycogen in the liver. In this respect glucagon is part of an *inflow controller*. Delta cells produce somatostatin, which inhibits both insulin and glucagon release. The most important disease of blood sugar regulation is diabetes mellitus when insulin secretion or its action is defective causing an excess of

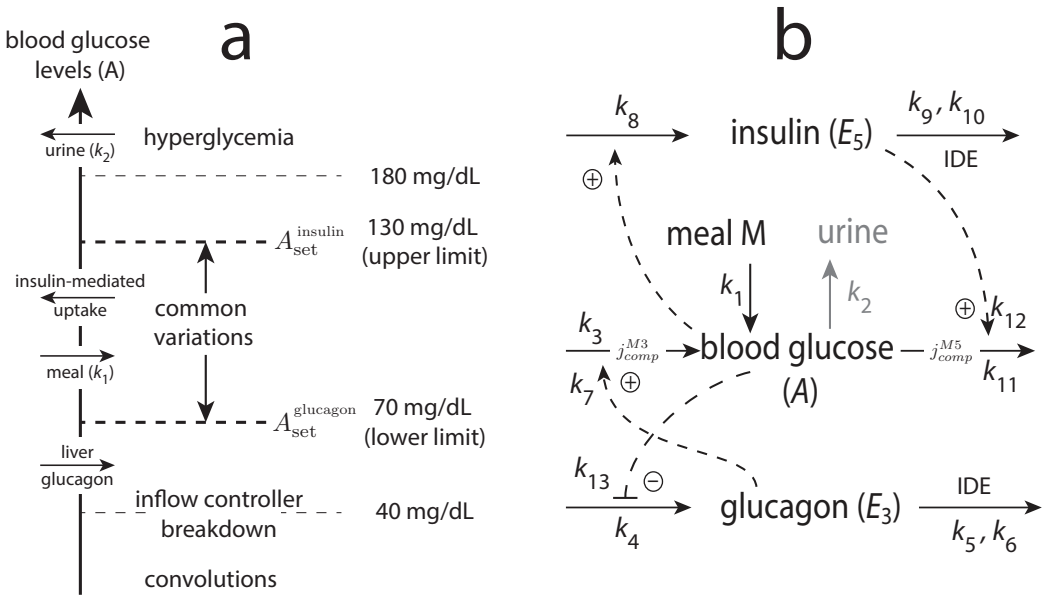

Figure 25: Blood glucose homeostasis described by a two-setpoint model. Panel a: Diagram of blood sugar levels based on Fig 1 in Cannon (1929). Common glucose variations, anticipated setpoints, glucose inflow/outflow fluxes, and areas of controller breakdown are indicated. $A_{set}^{glucagon}$ and $A_{set}^{insulin}$ are the respective setpoints of inflow and outflow controllers in panel b. Perturbation k_1 refers to the release of glucose by a meal. Since uptake of glucose into the organism's various tissues is dependent on insulin, k_2 is set to zero for healthy individuals. However, at high blood glucose levels glucose is excreted through the urine. The insulin-independent uptake of blood glucose by the kidneys and its recycling back into the blood stream is ignored. Glucagon activates the inflow of glucose into the blood by the liver when blood sugar levels are low. Panel b: Combined M3-M5 controller to describe blood glucose homeostasis. Degradations of insulin (E_5) and glucagon (E_1) are based on Michaelis-Menten kinetics by insulin degrading enzyme (IDE, insulysin). Compensatory flux j_{comp}^{M3} (see Table S25 in `Sup1.pdf`) refers to the glucagon-based inflow of glucose into the blood from the liver, while compensatory flux j_{comp}^{M5} is related to the insulin-based incorporation of glucose into various tissues such as muscles, skin and liver. When blood glucose levels are high some of the glucose is excreted through the urine (outlined in gray).

glucose in the blood (hyperglycemia).

In healthy individuals blood glucose is robustly regulated between about 70 mg/dL (4 mM) and 130 mg/dL (10 mM), but allows for variations within these limits (Fig 25a). Glucose levels which stay above 180 mg/dL or below 40 mg/dL will cause serious health problems (Kumar et al., 2013).

To test a two-setpoint model the M3-M5 combined controller is used as a candidate since these feedback structures are close to that of insulin and glucagon. Rate equations are found in Table S25 (`Sup1.pdf`) and in the M3-M5 part of `Sup2.pdf`. To avoid unrealistically high settling times as in the M1-M5 pair (see Fig 9) the isolated control mode ($A_{set}^{M5}{=}A_{set}^{insulin} > A_{set}^{M3}{=}A_{set}^{glucagon}$, Table 1, M3-M5, blue entry) is used. A represents blood glucose concentration, E_3 is glucagon, and E_5 refers to insulin (Fig 25b). Setpoints $A_{set}^{insulin}$ and $A_{set}^{glucagon}$

$$A_{set}^{insulin} = \frac{k_9}{k_8} \tag{45}$$

$$A_{set}^{glucagon} = \frac{k_4 k_{13} - k_5 k_{13}}{k_5} \tag{46}$$

are put to respectively 10 mM (130 mg/dL) and 4 mM (70 mg/dL) blood glucose. Although calculations will refer to blood glucose level in the mM range other parts of the model, i.e. hormone concentrations and the time scale still need to be considered as qualitative properties with arbitrary units. The generation of glucose from a taken meal M is formulated as a simple first-order reaction with respect to M (Fig 25b), i.e. the conversion of M into glucose is written as:

$$\text{conversion rate to glucose} = -\dot{M} = k_1 \cdot M \tag{47}$$

Fig 26 shows the influence of four parameters on blood glucose levels. Panel a indicates how different glucose release rates from a given meal M affect blood glucose profiles. The findings that a slower glucose release lowers the blood glucose amplitude after intake of the meal fits well with experimental results using continuous glucose profiles in nondiabetic individuals (see Fig 5 in Freckmann et al. (2007)).

Fig 26b shows the effect when insulin-based glucose incoorporation decreases (curves 1-4). The process involves an insulin-induced translocation of the glucose transporter GLUT4 Klip et al. (2019) to the cell surface such that glucose can enter the cell. Impairment of this process results in dysregulation of glucose homeostasis, insulin resistance (van Gerwen et al., 2023), and, as indicated in Fig 26b, to increased glucose levels.

An interesting prediction of the insulin (M5) part of the model is the increase of $A_{set}^{insulin}$ when production of insulin by decreased k_8 values is reduced (Fig 26c). Although glucose levels barely reach $A_{set}^{insulin}$ the insulin-related setpoint has a clear effect on the glucose amplitude after a meal.

Fig 26d shows the effect of different K_M values of the insulin degrading enzyme (IDE, insulysin). This K_M is of importance to define integral control and $A_{set}^{insulin}$ under ideal (low K_M) conditions (curves 1 and 2, see also section 2.5). As K_M increases robust perfect adaptation will be lost and controller accuracy decreases (Drengstig et al., 2012a). The enzyme data base BRENDA (`https://www.brenda-enzymes.org`) has listed about 20 K_M entries for IDE with respect to insulin binding. For all organisms, including human IDE, the listed K_M values are relative low and lie in the range between 1×10^{-5} mM to 1×10^{-4} mM. A K_M of 1×10^{-5} mM is roughly 10 times higher than the average post meal insulin concentration (2h after the meal), which has been measured to about 152 ± 31.7 μIU/mL$\approx 9\times10^{-7}$ mM (Shulka et al., 2015). This indicates that the binding between insulin and IDE is relative tight, but IDE's K_M is too high in comparison to insulin concentrations to obtain integral control/robust perfect adaptation as indicated by curves 1 or 2 in panel d. Curves 3-5 appear to be a more appropriate description for nondiabetic individuals.

In diabetics, ambulatory glucose profiles show occasional constant glucose levels (see Saturday 02 and 09 daily glucose profiles in Fig 1 of Johnson et al. (2019)), which may be interpreted that a setpoint has been reached when, due to medication, insulin levels have become tentatively higher than IDE's K_M. Since plateaus are also occasionally reached at lower glucose levels there appears to be a complex interplay between medication-induced insulin levels and related setpoint changes, and how fast glucose is generated from a meal.

The conclusion that is drawn from this relative simple model is: (i) There

appears to be two setpoints, each relating to insulin and glucagon based feedback loops. In nondiabetic individuals it is $A_{set}^{insulin}$ and $A_{set}^{glucagon}$ which are regulated. (ii) The adaptation to $A_{set}^{insulin}$ is not robustly perfect as glucose level are kept below $A_{set}^{insulin}$. The reason for this behavior is that insulin levels are lower than IDE's K_M. This allows for the incorporation of glucose into the organism's various tissues, but avoiding toxic blood glucose levels.

(iii) Diabetic individuals who have a lower insulin production rate will have a higher $A_{set}^{insulin}$ setpoint and blood glucose levels are therefore accordingly higher. However, an increased glucose setpoint may still be defended as ambulatory glucose profiles appear to indicate (Johnson et al., 2019). Medication, i.e. addition of insulin, will temporarily lower the setpoint.

4.2.1. Somatostatin

While insulin and glucagon are considered to be the main drivers of blood glucose homeostasis somatostatin (SST), which is released by pancreatic delta cells and certain neurons in the brain, is recognized as an additional regulator of blood glucose levels. Somatostatin is known to inhibit both insulin and glucagon, as well as many other regulatory peptides (Bloom and Polak, 1987). Due to its inhibitory role on both insulin and glucagon somatostatin should have an effect on the two setpoints determined by the insulin and glucagon negative feedback loops.

The rate equation for insulin (E_5) under steady state condition and SST inhibition can be written as

$$\dot{E_5} = k_8 \cdot A_{ss} \cdot \underbrace{\left(\frac{K_I^{SST}}{K_I^{SST}+SST}\right)}_{\text{somatostatin inhibition}} - k_9 \underbrace{\left(\frac{E_5}{k_{10}+E_5}\right)}_{\approx 1} = 0 \tag{48}$$

where K_I^{SST} is somatostatin's inhibition constant, SST denotes somatostatin concentration, and A_{ss}=$A_{set}^{insulin}$ describes the glucose setpoint by the insulin-based M5 feedback. Solving for A_{ss} we get

$$A_{ss} = A_{set}^{insulin} = \frac{k_9}{k_8}\left(1+\frac{SST}{K_I^{SST}}\right) \tag{49}$$

The influence of somatostatin inhibition on $A_{set}^{glucagon}$ can be described similarly by using the rate equation for glucagon (E_3), i.e.

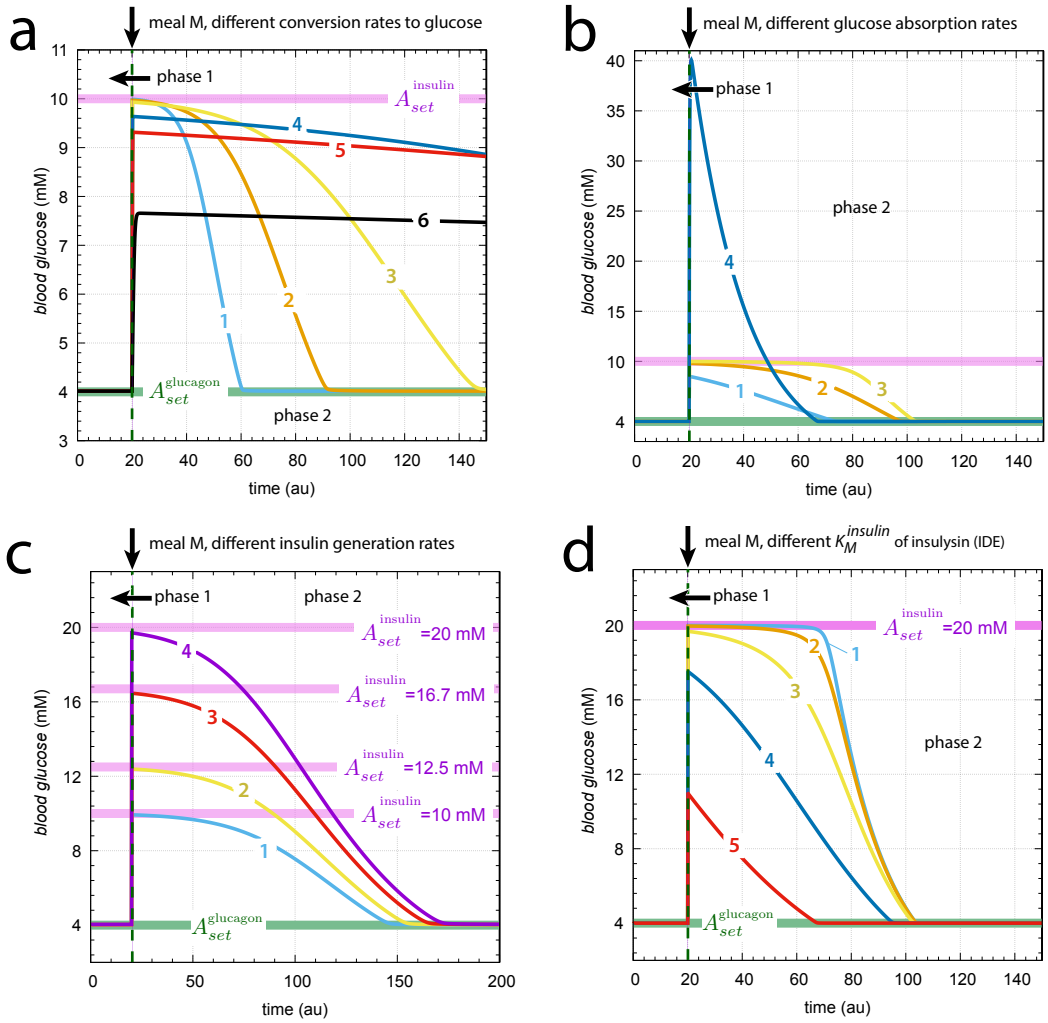

Figure 26: Parameters affecting blood glucose homeostasis in the M3-M5 model under isolated control. Panel a: Influence of a meal's glucose release rate (Eq 47) on blood glucose levels. Phase 1: fasting conditions with k_1=0.0. Starting phase 2 the meal is added at t=20 (vertical arrow) with an equivalent of 5M (5×10^3 mM) glucose. Curves 1-6 relate to k_1 values of respectively 0.2, 0.1, 0.05, 0.01, 0.005, and 0.001 inverse time units. Rate constants (phase 1 and phase 2): k_2=0.0, k_3=200.0, k_4=400.0, k_5=9.756098, k_6=1.0×10^{-6}, k_7=0.1, k_8=100.0, k_9=1.0×10^3, k_{10}=1.0×10^{-4}, k_{11}=200.0, k_{12}=k_{13}=0.1. Initial concentrations: A_0 (blood glucose)=4.0 mM, $E_{1,0}$ (glucagon)=2.7×10^{-4}, $E_{5,0}$ (insulin)=6.7×10^{-5}. Panel b: Influence of insulin-based glucose absorption rates j_{11} into the organism. Phase 1: fasting conditions with k_1=0.0 and k_2=1.0. Phase 2: k_1=0.05 (added meal), k_2=1.0. Curves 1-4 have k_{11} values of 5.0×10^3, 5.0×10^2, 50.0, and 5.0, respectively. Other rate constants and initial concentrations as in panel a. Panel c: Decrease of insulin generation rates increase insulin's glucose setpoint. Phase 1 as in panel a. Phase 2: Rate constants and initial concentrations as in panel a, except k_1=0.05. The k_8 values of curves 1-4 are 100.0, 80.0, 60.0, and 50.0, respectively. Insulin-based setpoints are calculated by Eq 45. Panel d: Influence of K_M^{IDE} (=k_{10}) of insulin degrading enzyme (IDE, insulysin) on blood glucose levels. Phases 1 and 2 as in panel b, except varying values of k_{10} (K_M^{IDE}), k_8=50.0, and k_{11}=200.0. Curves 1-5 have k_{10} values of 1.0×10^{-6}, 1.0×10^{-5}, 1.0×10^{-4}, 1.0×10^{-3}, and 1.0×10^{-2}, respectively. Other rate constants and initial concentrations as in panel b. See Python code for details.

$$\dot{E}_3 = k_4 \left(\frac{k_{13}}{k_{13}+A_{ss}} \right) \underbrace{\left(\frac{K_I^{SST}}{K_I^{SST}+SST} \right)}_{\text{somatostatin inhibition}} - k_5 \underbrace{\left(\frac{E_3}{k_6+E_3} \right)}_{\approx 1} = 0 \tag{50}$$

with $A_{set}^{glucagon}$ being

$$A_{set}^{glucagon} = A_{ss} = \frac{k_4 k_{13} K_I^{SST}}{k_5(K_I^{SST}+SST)} - k_{13} \tag{51}$$

Considering Eqs 49 and 51 we see that increased somatostatin levels should increase $A_{set}^{insulin}$, but decrease $A_{set}^{glucagon}$. Fig 27 shows the effect of increasing somatostatin levels on $A_{set}^{insulin}$ and $A_{set}^{glucagon}$.

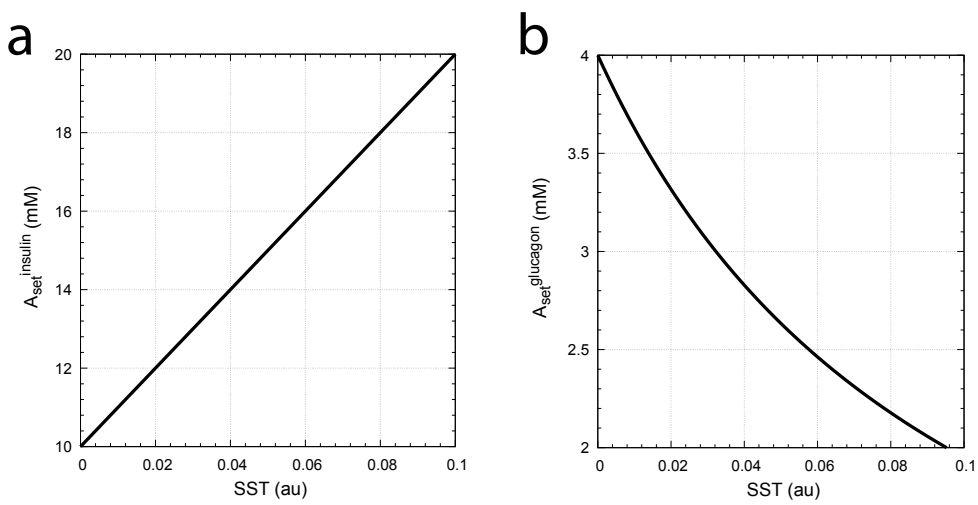

Figure 27: Increasing somatostatin levels (SST) lead to an increase and decrease of respectively $A_{set}^{insulin}$ and $A_{set}^{glucagon}$. Panels a and b show respectively Eq 49 and Eq 51. Parameter values are the same as in Fig 26 with additional K_I^{SSH}=0.1. K_I^{SSH} and SST levels are in arbitrary units.

The two-setpoint model thereby qualitatively predicts that under fasting conditions (blood sugar levels are determined by $A_{set}^{glucagon}$) a knockout of SST should lead to an increase in glucose steady states, while during non-fasting conditions (blood sugar levels are determined by $A_{set}^{insulin}$) a SST knockout should decrease $A_{set}^{insulin}$ and glucose levels.

Huang et al. (2024) indeed found that in non-fasting *Sst*-Cre$^{\mathrm{TG/TG}}$ mice (homozygous transgenic mice which do not express somatostatin) a significant decrease in steady state glucose levels is observed. The authors concluded that the (single) glycemic setpoint in absence of somatostatin is decreased.
Concerning the effect of somatostatin on basal glucose levels ($A_{set}^{glucagon}$) in fasting mice no direct results have been found in the literature. However, Xu et al. (2020) found that glucagon release from isolated perfused rat pancreas becomes high in presence of somatostatin blockers and that glucose lost its inhibitory effect on glucagon release in the presence of somatostatin blockers. Thus, somatostatin appears to be an essential part in the glucose-induced inhibition mechanism of glucagon release. As a consequence, basal glucose levels ($A_{set}^{glucagon}$) should increase when regulation by somatostatin is absent.

5. Summary and outlook

The subject of this work has been the study of two combined antagonistic (idealized) controllers with integral control which are (flatly) coupled through a common controlled variable A. The appearance of delegated and isolated control modes came to the author quite as a surprise. For each of the two control modes there are four instances with negative windup (blue entries in Table 1). As these combinations exhibit short settling times they appear to be good candidates to model antagonistic biochemical control systems. Whether metastable control or regulation by positive windup (yellow or red entries in Table 1 play a role in physiological regulation is not known.

Homeostatic systems are often considered to be related to single-loop negative feedbacks with only one setpoint. As shown by the above examples a possible way to understand rheostasis or antagonistic regulation like blood glucose is due to the interaction between two combined controllers. However, such an approach can be extended to include multiple feedbacks. For example, the use of three interlocked controller motifs (Ruoff and Nishiyama, 2020) can mimic the gradual change in p53 regulation for variable DNA-damaging stress. Although the p53 dynamics and the resulting setpoint and frequency changes are now quite complex, each of the three individual negative feedback controllers act as 'building blocks' in the overall homeostatic regulation of p53. Such an approach, i.e. the use of multiple combined controllers and how

they interact appears to be an interesting avenue to understand homeostatic regulation in Cannon's spirit.

Glossary

A brief description of the concepts used in the paper.

Controller or controller motif: A negative feedback arrangement.

Controlled variable: The variable which is under homeostatic control with one or several setpoints.

Controller variable or manipulated variable: The controller or manipulated variable generates a compensatory flux to oppose a perturbation applied on the controlled variable.

High affinity kinetics: In high affinity kinetics a catalyzing enzyme binds tightly to its substrate with a low Michaelis (dissociation) constant K_M.

IDE: Insulin degrading enzyme. Also named insulysin.

Integral control or integral feedback: In integral control the controller variable and its compensatory flux is related to the integrated error of the controller, i.e. the integrated difference between the actual value of the controlled variable (or a function of it) and the controller's setpoint (or a reference). Integral feedback leads to perfect adaptation to a controller's setpoint. Different kinetic mechanisms can result in integral control.

Low affinity kinetics: In low affinity kinetics a catalyzing enzyme binds loosely to its substrate with a large Michaelis (dissociation) constant K_M. Resembles often first-order or close to first-order kinetics.

Relaxation or settling time: The time to reach a steady state after a perturbation has been applied.

Reaction order: In a rate equation, the reaction order with respect to a chemical species is the exponent for that species.

Steady state: The steady state of a compound A is reached when its concentration does not change, i.e. the time derivative $\mathrm{d}A/\mathrm{d}t = \dot{A} = 0$.

SST: Somatostatin.

Windup: The continuous increase or decrease of a controller variable.

Supplementary material

`Sup1.pdf:` The file provides an overview of setpoints, windup properties, and borderlines for all 16 controller combinations in both delegated and isolated control mode.

`Sup2.pdf:` A detailed description of setpoints, delegated and isolated control modes, and borderlines for the M2-M7, M3-M5, and M4-M8 combined controllers.

`Sup3.pdf:` Additional examples of metastable control.

`Sup4.mp4:` Influence of k_3 on phase diagram in delegated control mode (all controller combinations).

`Sup5.mp4:` Influence of k_3 on phase diagram in isolated control mode (all controller combinations).

`Sup6.mp4:` Influence of k_{11} on phase diagram in delegated control mode (all controller combinations).

`Sup7.mp4:` Influence of k_{11} on phase diagram in isolated control mode (all controller combinations).

`Python codes:` A selected set of results in Python code.

Funding sources

This research did not receive any specific grant from funding agencies in the public, commercial, or not-for-profit sectors.

References

Andrews, S.S., Kochen, M., Smith, L., Feng, S., Wiley, H.S., Sauro, H.S., 2024. Signal integration and integral feedback control with biochemical reaction networks. bioRxiv doi:https://doi.org/10.1101/2024.04.26.591337.

Ang, J., Bagh, S., Ingalls, B., McMillen, D., 2010. Considerations for using integral feedback control to construct a perfectly adapting synthetic gene network. J Theor Biol 266, 723–738.

Ang, J., McMillen, D., 2013. Physical Constraints on Biological Integral Control Design for Homeostasis and Sensory Adaptation. Biophys J 104, 505–515.

Aoki, S.K., Lillacci, G., Gupta, A., Baumschlager, A., Schweingruber, D., Khammash, M., 2019. A universal biomolecular integral feedback controller for robust perfect adaptation. Nature 570, 533–537.

Araujo, R.P., Liotta, L.A., 2018. The topological requirements for robust perfect adaptation in networks of any size. Nature Communications 9, 1757.

Araujo, R.P., Liotta, L.A., 2023. Universal structures for adaptation in biochemical reaction networks. Nature Communications 14, 2251.

Bao, R., Onishi, K.G., Tolla, E., Ebling, F.J., Lewis, J.E., Anderson, R.L., Barrett, P., Prendergast, B.J., Stevenson, T.J., 2019. Genome sequencing and transcriptome analyses of the siberian hamster hypothalamus identify mechanisms for seasonal energy balance. PNAS 116, 13116–13121.

Barkai, N., Leibler, S., 1997. Robustness in simple biochemical networks. Nature 387, 913–7.

Bartness, T.J., Wade, G.N., 1985. Photoperiodic control of seasonal body weight cycles in hamsters. Neuroscience & Biobehavioral Reviews 9, 599–612.

Bhattacharya, P., Raman, K., Tangirala, A.K., 2024. Design principles for perfect adaptation in biological networks with nonlinear dynamics. Bulletin of Mathematical Biology 86, 100.

Billman, G.E., 2020. Homeostasis: The underappreciated and far too often ignored central organizing principle of physiology. Frontiers in Physiology 11, 200.

Blanchini, F., Cuba Samaniego, C., Franco, E., Giordano, G., 2018. Homogeneous time constants promote oscillations in negative feedback loops. ACS Synthetic Biology 7, 1481–1487.

Bloom, S., Polak, J., 1987. Somatostatin. British Medical Journal (Clinical Research Ed.) 295, 288.

Bosdriesz, E., Wortel, M.T., Haanstra, J.R., Wagner, M.J., De La Torre Cortes, P., Teusink, B., 2018. Low affinity uniporter carrier proteins can increase net substrate uptake rate by reducing efflux. Scientific Reports 8, 1–9.

Briat, C., Zechner, C., Khammash, M., 2016. Design of a synthetic integral feedback circuit: dynamic analysis and dna implementation. ACS Synthetic Biology 5, 1108–1116.

Cannon, W., 1929. Organization for Physiological Homeostasis. Physiol. Rev. 9, 399–431.

Cannon, W., 1939. The Wisdom of the Body. Revised and Enlarged Edition. Norton, New York.

Cannon, W.B., 1926. Physiological regulation of normal states: Some tentative postulates concerning biological homeostatics. Selected Readings in the History of Physiology , 329–332.

Carpenter, R., 2004. Homeostasis: A plea for a unified approach. Advances in Physiology Education 28, 180–187.

Clancy, J., McVicar, A.J., 2002. Physiology and Anatomy. A Homeostatic Approach. Second edition. Arnold.

Cornish-Bowden, A., 2004. Fundamentals of Enzyme Kinetics. Third Edition. Portland Press, London.

Curtis, H., Koshland, M., Nims, L., Quastler, H., 1958. Homeostatic Mechanisms. Brookhaven Symposia in Biology, Number 10. Brookhaven National Laboratory, Upton, New York.

De Paula, R., Vitalini, M., Gomer, R., Bell-Pedersen, D., 2007. Complexity of the *Neurospora crassa* circadian clock system: Multiple loops and oscillators, in: Cold Spring Harbor Symposia on Quantitative Biology, Cold Spring Harbor Laboratory Press. pp. 345–351.

Drengstig, T., Jolma, I., Ni, X., Thorsen, K., Xu, X., Ruoff, P., 2012a. A basic set of homeostatic controller motifs. Biophys J 103, 2000–2010.

Drengstig, T., Ni, X., Thorsen, K., Jolma, I., Ruoff, P., 2012b. Robust adaptation and homeostasis by autocatalysis. J Phys Chem B 116, 5355–5363.

Drengstig, T., Ueda, H., Ruoff, P., 2008. Predicting Perfect Adaptation Motifs in Reaction Kinetic Networks. J Phys Chem B 112, 16752–16758.

Dunlap, J., 1999. Molecular bases for circadian clocks. Cell 96, 271–290.

Farnsworth, K.D., 2025. Homeostatic set-points are physical and foundational to organism autonomy. BioSystems , 105634.

Fjeld, G., Thorsen, K., Drengstig, T., Ruoff, P., 2017. Performance of homeostatic controller motifs dealing with perturbations of rapid growth and depletion. J Phys Chem B 121, 6097–6107.

Franck, U., 1980. Feedback Kinetics in Physicochemical Oscillators. Berichte der Bunsengesellschaft für Physikalische Chemie 84, 334–41.

Freckmann, G., Hagenlocher, S., Baumstark, A., Jendrike, N., Gillen, R.C., Rössner, K., Haug, C., 2007. Continuous glucose profiles in healthy subjects under everyday life conditions and after different meals. Journal of Diabetes Science and Technology 1, 695–703.

Frieden, C., 1970. Kinetic aspects of regulation of metabolic processes: The hysteretic enzyme concept. Journal of Biological Chemistry 245, 5788–5799.

van Gerwen, J., Shun-Shion, A.S., Fazakerley, D.J., 2023. Insulin signalling and glut4 trafficking in insulin resistance. Biochemical Society Transactions 51, 1057–1069.

Goldbeter, A., Gonze, D., Houart, G., Leloup, J.C., Halloy, J., Dupont, G., 2001. From simple to complex oscillatory behavior in metabolic and genetic control networks. Chaos: An Interdisciplinary Journal of Nonlinear Science 11, 247–260.

Goodwin, B., 1963. Temporal Organization in Cells. Academic Press, London.

Helfrich-Förster, C., 2009. Does the morning and evening oscillator model fit better for flies or mice? Journal of Biological Rhythms 24, 259–270.

Hirono, Y., Gupta, A., Khammash, M., 2025. Rethinking robust adaptation: Characterization of structural mechanisms for biochemical network robustness through topological invariants. PRX Life 3, 013017.

Hirono, Y., Hong, H., Kim, J.K., 2023. Robust perfect adaptation of reaction fluxes ensured by network topology. arXiv:2302.01270 doi:https://doi.org/10.48550/arXiv.2302.01270.

Hochachka, P.W., Somero, G.N., 1984. Biochemical Adaptation. Princeton University Press.

Huang, J.L., Pourhosseinzadeh, M.S., Lee, S., Krämer, N., Guillen, J.V., Cinque, N.H., Aniceto, P., Momen, A.T., Koike, S., Huising, M.O., 2024. Paracrine signaling by pancreatic δ cells determines the glycemic set point in mice. Nature Metabolism 6, 61–77.

Huang, Y., Drengstig, T., Ruoff, P., 2011. Integrating fluctuating nitrate uptake and assimilation to robust homeostasis. Plant, Cell and Environment 35, 917–928.

Hughes, G., 1964. Homeostasis and Feedback Mechanisms. Academic Press, New York.

Iglesias, P.A., Ingalls, B.P., 2010. Control Theory and Systems Biology. MIT Press.

Illnerová, H., 1991. The suprachiasmatic nucleus and rhythmic pineal melatonin production, in: Klein, David C. and Moore, Robert Y. and Reppert, Stephen M. (Ed.), Suprachiasmatic Nucleus: The Mind's Clock. Oxford University Press, New York, pp. 197–216.

Jagota, A., de la Iglesia, H.O., Schwartz, W.J., 2000. Morning and evening circadian oscillations in the suprachiasmatic nucleus *in vitro*. Nature Neuroscience 3, 372–376.

Johnson, M.L., Martens, T.W., Criego, A.B., Carlson, A.L., Simonson, G.D., Bergenstal, R.M., 2019. Utilizing the ambulatory glucose profile to standardize and implement continuous glucose monitoring in clinical practice. Diabetes Technology & Therapeutics 21, S2–17–S2–25.

Jolma, I., Ni, X., Rensing, L., Ruoff, P., 2010. Harmonic Oscillations in Homeostatic Controllers: Dynamics of the p53 Regulatory System. Biophys J 98, 743–752.

Khammash, M.H., 2021. Perfect adaptation in biology. Cell Systems 12, 509–521.

Kholodenko, B.N., 2000. Negative feedback and ultrasensitivity can bring about oscillations in the mitogen-activated protein kinase cascades. European Journal of Biochemistry 267, 1583–1588.

Klip, A., McGraw, T.E., James, D.E., 2019. Thirty sweet years of glut4. Journal of Biological Chemistry 294, 11369–11381.

Krishnan, J., Floros, I., 2019. Adaptive information processing of network modules to dynamic and spatial stimuli. BMC Systems Biology 13, 1–26.

Kumar, V., Abbas, A.K., Aster, J.C., 2013. Robbins Basic Pathology. 9th Edition. Elsevier Saunders.

Langley, L.L., 1973. Homeostasis. Origins of the Concept. Dowden, Hutchinson & Ross, Inc., Stroudsbourg, Pennsylvania.

Levchenko, A., Iglesias, P.A., 2002. Models of eukaryotic gradient sensing: application to chemotaxis of amoebae and neutrophils. Biophys J 82, 50–63.

Lloyd, D., Aon, M., Cortassa, S., 2001. Why homeodynamics, not homeostasis? The Scientific World 1, 133–145.

M. Zand, A., Anastassov, S., Frei, T., Khammash, M., 2024. Multi-layer autocatalytic feedback enables integral control amidst resource competition and across scales. ACS Synthetic Biology .

Mangum, C., Towle, D., 1977. Physiological adaptation to unstable environments: Inconstancy of the internal milieu in an animal may be a regulatory mechanism. American Scientist 65, 67–75.

Moore-Ede, M., 1986. Physiology of the circadian timing system: Predictive versus reactive homeostasis. Am. J. Physiol. 250, R737–52.

Morse, D., Hastings, J.W., Roenneberg, T., 1994. Different phase responses of the two circadian oscillators in *Gonyaulax*. Journal of Biological Rhythms 9, 263–274.

Mrosovsky, N., 1990. Rheostasis. The Physiology of Change. Oxford University Press, New York.

Ni, X., Drengstig, T., Ruoff, P., 2009. The control of the controller: Molecular mechanisms for robust perfect adaptation and temperature compensation. Biophys J 97, 1244–53.

Nishiyama, N., Ruoff, P., Jimenez, J.C., Miwakeichi, F., Nishiyama, Y., Yata, T., 2023. Modeling the interaction between donor-derived regulatory t cells and effector t cells early after allogeneic hematopoietic stem cell transplantation. Biosystems 227, 104889.

Nygård, M., Ruoff, P., 2023. Coherent feedback leads to robust background compensation in oscillatory and non-oscillatory homeostats. PLoS One 18, e0287083.

Pigolotti, S., Krishna, S., Jensen, M.H., 2007. Oscillation patterns in negative feedback loops. PNAS 104, 6533–6537.

Pittendrigh, C.S., Daan, S., 1976. A functional analysis of circadian pacemakers in nocturnal rodents: V. Pacemaker structure: A clock for all seasons. Journal of Comparative Physiology 106, 333–355.

Ponsiglione, A.M., Montefusco, F., Donisi, L., Tedesco, A., Cosentino, C., Merola, A., Romano, M., Amato, F., 2023. A general approach for the modelling of negative feedback physiological control systems. Bioengineering 10, 835.

Radhakrishnan, K., Hindmarsh, A., 1993. Description and Use of LSODE, the Livermore Solver for Ordinary Differential Equations. NASA Reference Publication 1327, Lawrence Livermore National Laboratory Report UCRL-ID-113855. National Aeronautics and Space Administration, Lewis Research Center, Cleveland, OH 44135-3191.

Rensing, L., Mohsenzadeh, S., Ruoff, P., Meyer, U., 1997. Temperature Compensation of the Circadian Period Length-A Special Case Among General

Homeostatic Mechanisms of Gene Expression? Chronobiology International 14, 481–498.

Ruoff, P., Nishiyama, N., 2020. Frequency switching between oscillatory homeostats and the regulation of p53. PloS One 15, e0227786.

Saito, K., Yamauchi, T., Hiraike, Y., 2025. Circadian regulation of metabolic homeostasis in physiology and disease. The Journal of Biochemistry , mvaf084.

Saunders, P., Koeslag, J., Wessels, J., 1998. Integral rein control in physiology. J Theor Biol 194, 163–173. doi:10.1006/jtbi.1998.0746.

Saunders, P., Koeslag, J., Wessels, J., 2000. Integral rein control in physiology II: A general model. J 206, 211–220. doi:10.1006/jtbi.2000.2118.

Schulkin, J., 2003. Rethinking Homeostasis. Allostatic Regulation in Physiology and Pathophysiology. MIT Press, Cambridge, Massachusetts.

Schulkin, J., 2004. Allostasis, Homeostasis and the Costs of Physiological Adaptation. Cambridge University Press, Cambridge, Massachusetts.

Segel, I.H., 1975. Enzyme Kinetics. Behavior and Analysis of Rapid Equilibrium and Steady State Enzyme Systems. Wiley, New York.

Selye, H., 1974. Stress without Distress. J. B Lippincott Company, Philadelphia & New York, New York.

Shinar, G., Feinberg, M., 2010. Structural sources of robustness in biochemical reaction networks. Science 327, 1389–1391.

Shoval, O., Goentoro, L., Hart, Y., Mayo, A., Sontag, E., Alon, U., 2010. Fold-change detection and scalar symmetry of sensory input fields. PNAS 107, 15995–16000.

Shulka, A.P., Iliescu, R.G., Thomas, C.E., Aronne, L.J., 2015. Food order has a significant impact on postprandial glucose and insulin levels. Diabetes Care 38, e98–9.

Sterling, P., Eyer, J., 1988. Allostasis: A new paradigm to explain arousal pathology, in: Fisher, S. and Reason, J. (Ed.), Handbook of Life Stress, Cognition and Health. John Wiley & Sons, New York, pp. 629–49.

Stevenson, T.J., 2024. On Rheostasis. The Hierarchical Organization of Physiological Stability. Oxford University Press.

Stoleru, D., Nawathean, P., de la Paz Fernández, M., Menet, J.S., Ceriani, M.F., Rosbash, M., 2007. The drosophila circadian network is a seasonal timer. Cell 129, 207–219.

Thorsen, K., Agafonov, O., Selstø, C.H., Jolma, I.W., Ni, X.Y., Drengstig, T., Ruoff, P., 2014. Robust concentration and frequency control in oscillatory homeostats. PLoS One 9(9), e107766. doi:10.1371/journal.pone.0107766.

Thorsen, K., Ruoff, P., Drengstig, T., 2018. Antagonistic regulation with a unique setpoint, integral and double integral action. bioRxiv URL: `https://doi.org/10.1101/248682`, doi:10.1101/248682.

Warwick, K., 1996. An Introduction to Control Systems. Second Edition. World Scientific.

Wilkie, J., Johnson, M., Reza, K., 2002. Control Engineering. An Introductory Course. Palgrave, New York.

Xu, S.F., Andersen, D.B., Izarzugaza, J.M., Kuhre, R.E., Holst, J.J., 2020. In the rat pancreas, somatostatin tonically inhibits glucagon secretion and is required for glucose-induced inhibition of glucagon secretion. Acta Physiologica 229, e13464.

Yi, T., Huang, Y., Simon, M., Doyle, J., 2000. Robust perfect adaptation in bacterial chemotaxis through integral feedback control. PNAS 97, 4649–53.